Two plastidial lysophosphatidic acid acyltransferases differentially mediate the biosynthesis of membrane lipids and triacylglycerols in Phaeodactylum tricornutum

Lingjie You, Ada Polońska, Katarzyna Jasieniecka-Gazarkiewicz, Fabien Richard, Juliette Jouhet, Eric Maréchal, Antoni Banaś, Hanhua Hu, Yufang Pan, Xiahui Hao, et al.

Two plastidial lysophosphatidic acid acyltransferases differentially mediate the biosynthesis of membrane lipids and triacylglycerols in *Phaeodactylum tricornutum*

Lingjie You[1], Ada Połońska[2], Katarzyna Jasieniecka-Gazarkiewicz[2], Fabien Richard[3], Juliette Jouhet[3] (ORCID https://orcid.org/0000-0002-4402-2194), Eric Maréchal[3] (ORCID https://orcid.org/0000-0002-0060-1696), Antoni Banaś[2], Hanhua Hu[4] (ORCID, https://orcid.org/0000-0002-8485-7591), Yufang Pan[4], Xiahui Hao[1], Hu Jin[5], Andrew E. Allen[6,7] (ORCID, https://orcid.org/0000-0001-5911-6081), Alberto Amato[3] (ORCID, https://orcid.org/0000-0002-9126-5535), Yangmin Gong[1,8] (ORCID, https://orcid.org/0000-0002-4096-3640)

[1]Oil Crops Research Institute of the Chinese Academy of Agricultural Sciences, Wuhan 430062, China;
[2]Intercollegiate Faculty of Biotechnology of UG and MUG, Gdansk, Poland
[3]Laboratoire de Physiologie Cellulaire et Végétale; Centre National de la Recherche Scientifique, Commissariat à l'Energie Atomique et aux Energies Alternatives; INRAE; Université Grenoble Alpes, Unité mixte de recherche 5168, IRIG, CEA Grenoble, F-38041 Grenoble, France;
[4]Key Laboratory of Algal Biology, Institute of Hydrobiology, Chinese Academy of Sciences, Wuhan 430072, China;
[5] Center for Microalgal Biotechnology and Biofuels, Institute of Hydrobiology, Chinese Academy of Sciences, Wuhan 430072, China.
[6]Scripps Institution of Oceanography, University of California, San Diego, La Jolla, CA 92093, USA;
[7]J. Craig Venter Institute, 4120 Capricorn Lane, La Jolla, CA 92037, USA
[8]Key Laboratory of Biology and Genetic Improvement of Oil Crops, Ministry of Agriculture, Oil Crops Research Institute of Chinese Academy of Agricultural Sciences, Wuhan 430062, China;

Author for correspondence:
Yangmin Gong
Tel: +86-27-86711526
E-mail: gongyangmin@caas.cn

Alberto Amato
Tel: +33 (0)4 38 78 44 93
E-mail: Alberto.AMATO@cea.fr

Total word count (excluding summary, references and legends):	6316	No. of figures:	10
Summary:	197	No. of Tables:	0
Introduction:	1083	No. of Supporting Information files:	3 (Fig.S1-5,Table S1-S2; Dataset S1; Methods S1)
Materials and Methods:	1073		
Results:	2683		
Discussion:	1310		
Acknowledgements:	167		

Summary

- Lysophosphatidic acid acyltransferases (LPAATs) catalyze the formation of phosphatidic acid, a central metabolite in both prokaryotic and eukaryotic organisms for glycerolipid biosynthesis. *Phaeodactylum tricornutum* contains at least two plastid-localized LPAATs (ptATS2a and ptATS2b), but their roles in lipid synthesis remain unknown.
- Both ptATS2a and ptATS2b could complement the high temperature sensitivity of the bacterial *plsC* mutant deficient in LPAAT. *In vitro* enzyme assays showed that they prefer lysophosphatidic acid over other lysophospholipids.
- ptATS2a is localized in the plastid inner envelope membrane and CRISPR/Cas9-generated *ptATS2a* mutants showed compromised cell growth, significantly changed plastid and extra-plastidial membrane lipids at nitrogen-replete condition and reduced triacylglycerols (TAGs) under nitrogen-depleted condition. ptATS2b is localized in thylakoid membranes and its knockout led to reduced growth rate and TAG content but slightly altered molecular composition of membrane lipids.
- The changes of glycerolipid profiles are consistent with the role of both LPAATs in the *sn*-2 acylation of *sn*-1-acyl-glycerol-3-phosphate substrates harboring 20:5 at the *sn*-1 position. Our findings suggest that both LPAATs are important for membrane lipids and TAG biosynthesis in *P. tricornutum*, and further highlight that 20:5-Lyso-PA is likely involved in the massive import of 20:5 back to the plastid to feed plastid glycerolipid syntheses.

Key words: Chloroplast membrane lipids, Lysophosphatidic acid acyltransferase, Multiplexed CRISPR/Cas9, *Phaeodactylum tricornutum*, Triacylglycerol.

Introduction

Phosphatidic acid (PA) and its dephosphorylated form, diacylglycerol (DAG) are key precursors for the biosynthesis of membrane glycerolipids and the storage lipid triacylglycerol (TAG) (Miège and Maréchal, 1999; Okazaki et al. 2006). PA is generated predominantly through two steps of acylation reactions at the *sn*-1 and *sn*-2 positions of glycerol-3-phosphate (G3P), which are catalyzed by G3P acyltransferase (GPAT; EC 2.3.1.15) and lysophosphatidic acid acyltransferase (LPAAT; EC 2.3.1.51). In the second reaction, LPAAT transfers an acyl group to the *sn*-2 position of lysophosphatidic acid (lysoPA) to produce PA and is essential to PA synthesis in almost all cellular organisms.

In *Escherichia coli*, *plsC* encodes the sole LPAAT catalyzing the conversion of lysoPA to form PA, which is then utilized as substrate for synthesis of membrane phospholipids consisting mainly of phosphatidylethanolamine (PE), phosphatidylglycerol (PG) and cardiolipin (CL). The *plsC*-deficient mutant is non-permissive for cell growth when temperature was elevated (Cullinane et al. 2005). In the yeast *Saccharomyces cerevisiae*, *SLC1*, together with *SLC4*, encodes partially redundant LPAAT activity. The *slc1Δslc4Δ* double knockout mutant is lethal, suggesting an essential role of LPAAT activity in yeast.

In higher plants, FAs serving as building blocks for all membrane lipids and TAG are exclusively synthesized in the stroma of chloroplasts. Then, two parallel pathways operate for the biosynthesis of chloroplast thylakoid lipids, one localized within the plastid, and the other in the endoplasmic reticulum (ER) (Roughan and Slack, 1982). A portion of the *de novo*-synthesized FAs can be directly used in the chloroplast for successive acylation of G3P to produce lysoPA and PA, catalyzed by a plastid acyl-acyl carrier protein (ACP):G3P acyltransferase encoded by *ATS1* (Kunst et al. 1988; Xu et al. 2006) and a plastid LPAAT encoded by *ATS2* (Kim and Huang 2004), respectively. PA is subsequently dephosphorylated in the chloroplast to generate DAG, both serving as precursors for synthesis of the predominant thylakoid membrane lipids, mainly PG from PA via a CDP-DAG intermediate, and monogalactosyldiacylglycerol (MGDG), digalactosyldiacylglycerol (DGDG) and sufoquinovosyldiacylglycerol (SQDG), from DAG. This chloroplast pathway is referred to as the "prokaryotic pathway". In parallel, FAs synthesized in the chloroplast can also be exported to the cytosol and assembled into extra-plastidial membrane glycerolipids and TAG at the ER. G3P in the ER is sequentially esterified to generate lysoPA and PA by membrane-bound acyl-CoA:G3P acyltransferase and LPAAT using acyl-CoA as FA donor, respectively. In this so-called "eukaryotic

pathway", PA generated in the ER is dephosphorylated into DAG, which serves as substrate for the formation of extra-plastidial membrane lipids and TAGs (Benning 2008). In many plants, there is a large flux of glycerolipids between the ER and chloroplast, as lipid precursors assembled at the ER can find their way back to the chloroplast feeding the biosynthesis of thylakoid membrane lipids (Xu et al. 2008). It was found that the prokaryotic pathway operating in the chloroplast produces glycerolipids containing mainly 16-carbon (C16) FAs at the *sn*-2 position of DAG backbone, while the same position of glycerolipids synthesized by the ER-located eukaryotic pathway is exclusively occupied by C18 FAs (Heinz and Roughan 1983). This difference in acyl composition of lipids has been observed in many plants and is substantially determined by the distinct substrate specificities and functions of LPAATs or acyl exchange enzymes in the plastid and the ER (Awai et al. 2006).

The diatom *Phaeodactylum tricornutum*, a unicellular photoautotrophic microalga with a sequenced genome, is known to produce the ω-3 long-chain polyunsaturated FA, eicosapentaenoic acid (EPA, $20{:}5\Delta^{5,8,11,14,17}$). Under nutrient stress, *P. tricornutum* accumulates large amounts of TAGs stored in lipid droplet. Diatoms usually have a plastid surrounded by a four-layered membrane system. The outermost two membranes are known as the 'epiplastidial membrane' or 'chloroplast ER' (cER), possibly deriving from a phagocytic membrane, and the 'periplastidial membrane' (PPM) and two innermost membranes corresponding to the 'classical' chloroplast envelope (Grosche et al., 2014; Petroutsos et al., 2014).

The thylakoid membrane lipids from *P. tricornutum* differ strongly from plant lipids. The extremely high proportion of 20:5 at position *sn*-1 in MGDG, DGDG or SQDG (Abida et al, 2015), a FA initially generated in the cytosol (Dolch and Marechal, 2015; Dolch et al, 2017) indicates its massive import back to the plastid, *via* an elusive route tentatively named the 'omega pathway' (Petroutsos et al, 2014). At the *sn*-2 position, MGDG, DGDG and SQDG contain mainly C16 FAs, suggesting that plastid-targeted LPAATs (ATS2s) have very strong preference for a C16-ACP as reported in higher plants (Frentzen et al., 1983). For example, under the nutrient-replete condition the *sn*-2 position of MGDG is exclusively esterified to 16:3 whereas the same position of DGDG is mainly occupied by 16:1 and 16:2. By contrast, storage TAGs that are thought to be assembled at the ER mostly have 16:0 and 16:1 esterified at the *sn*-2 position of their glycerol backbone, indicating that ER-located LPAAT from diatoms may have a preference for C16 similar to that of plastid ATS2(s) as it was also shown in *Chlamydomonas reinhardtii* (Kim et al., 2018). The substrate specificity of the ER

LPAAT would thus differ from that of LPAATs characterized in most land plants. Eventually, *P. tricornutum* may lack specific signature that could support the existence of a potential eukaryotic pathway providing diacyl precursors for the synthesis of chloroplast membrane lipids. Indeed, in plants, PA and DAG have been suggested as the species transported from the ER to the chloroplast, *via* this eukaryotic pathway, for MGDG synthesis (Slack et al., 1977; Xu et al., 2005; Lu and Benning, 2009; Karki et al., 2019). In *P. tricornutum*, whether there is a transfer of a diacyl-moiety such as PA/DAG from extra-plastidic phospholipids to feed galactoglycerolipid synthesis is still unknown.

The understanding of lipid biosynthesis in diatoms and our ability to genetically manipulate some oleaginous species to produce oils with tailored FA composition and increased TAG content, await the identification of key enzymes. In the diatom *P. tricornutum*, several acyltransferases involved in TAG synthesis have been reported and intracellular TAG content could be enhanced by overexpression of a glycerol-3-phosphate acyltransferase, or a type 2 diacylglycerol acyltransferase (Niu et al. 2016; Haslam et al. 2020; Wang et al. 2020; You et al. 2023). In this study, we identified Phatr3_J11916 and Phatr3_J43099 as plastid-localized LPAATs in *P. tricornutum*. We characterized their LPAAT activities by heterologous expression in bacterial and yeast mutants and determined their subcellular localization. We further generated single mutants using multiplexed CRISPR/Cas9 method and characterized their lipid-associated phenotypes under different conditions with high-resolution lipidomics approaches. We then characterized their roles in membrane and storage glycerolipid homeostasis in *P. tricornutum*.

Materials and methods

A detailed method section, including plasmid construction, *in vitro* enzyme assay, generation of *ptATS2* mutants, photosynthetic measurement and glycerolipid extraction and analysis, is presented in Supporting Information Methods S1.

Microbial strains and growth conditions

Escherichia coli DH5α or EPI300 strain was grown at 37°C in Luria Broth (LB) supplemented with appropriate antibiotics (ampicillin 50 mg L^{-1} or gentamycin 10 mg L^{-1} or tetracyclin 20 mg L^{-1}). *E. coli plsC*Δ mutant SM2-1 was grown in LB without antibiotic and the complementation strains harboring the empty vector pQE60 or expressing ptATS2a/2b were grown in LB supplemented with 50 mg L^{-1} ampicillin at 37°C or 42°C. *Phaeodactylum tricornutum* Bohlin (CCMP 2561) from the culture collection of the Provasoli-Guillard National Center for Culture of Marine Phytoplankton (Bigelow

Laboratory for Ocean Sciences, East Boothbay, ME) was grown in artificial sea water enriched with f/2 medium (Guillard 1975), at 22°C under cool white fluorescence lights (75 μE m^{-2} s^{-1}) and a photoperiod of 12 h light: 12 h dark. The *P. tricornutum ptATS2a* and *ptATS2b* mutants were grown in f/2 medium supplemented with appropriate antibiotics (zeocin 50 mg L^{-1} or nourseothricin 100 mg L^{-1}). For the cell growth experiments reported in Fig.5a-h, 600 mL of algal cultures of wild type and mutants were grown in 1 L flasks with bubbling of filtered air for 12 days at 22°C in a temperature-controlled incubator. In addition, 300 mL of algal cells were grown in 500 mL flasks for 18 days in static culture. In both conditions, algal cultures were inoculated using cultures in exponential phase (1-2×10^6 cells/mL) to the same initial cell concentration of approximately 5×10^4 cells/mL and illuminated continuously from ~ 50 μE m^{-2} s^{-1} cool white fluorescence lights. For the cell growth experiments reported in Fig.5i-l, N-starved cultures were prepared by centrifuging from cultures in exponential phase (1-2×10^6 cells/mL) and washing cells twice in the N-free f/2 media and then resuspending them in N-free media for 4 days. Approximately 5 mL of algal cultures were sampled daily and monitored for cell concentration and nitrate concentration in the media which was measured spectrophotometrically at 220 nm (Collos et al. 1999). The nonpolar lipid content was evaluated by fluorometric assay using the dye Nile Red (Sigma-Aldrich). A total of 6×10^6 cells for each sample were stained with Nile Red and the fluorescence was measured at 572 nm using an F-7000 Fluorescence Spectrophotometer (HITACHI, Japan).

Generation of ptATS2a/2b-GFP fusion transgenic strains and fluorescence microscopy

The plasmids carrying ptATS2a-GFP or ptATS2b-GFP fusion were introduced into *P. tricornutum* cells by microparticle bombardment using the Bio-Rad Biolistic PDS-1000/He Particle Delivery System (Bio-Rad) as described by Zaslavskaia et al. (2000). The zeocin-resistant clones were subjected to a screening based on the observation of detectable GFP fluorescence signals. Subcellular localization of GFP fusion proteins were examined by laser scanning confocal microscopy (Leica SP8).

Generation of *P. tricornutum ptATS2a*/*ptATS2b* mutants

The CRISPR/Cas9-episome plasmids harboring multiple sgRNA expression cassettes were transformed into *P. tricornutum* by bacterial conjugation as described by Karas et al. (2015). After 10-14 days, colonies were directly transferred into liquid f/2 media containing 100 μg mL^{-1} zeocin in a 48-well plate. The genomic DNA was isolated from each clone and the genomic regions spanning the predicted Cas9 targeting sites were amplified and subjected for DNA sequencing. The Inference of CRISPR

Edits tool (ICE, Synthego, https://ice.synthego.com) was used to analyze indels resulting from Cas9 targeting of *ptATS2a* or *ptATS2b* by multiple sgRNAs. *P. tricornutum* transformed with the Cas9-2A-sh ble empty vector was used as control strains. Colonies carrying mutations with indel percentage >90% and Knockout Score >90 were selected and grown in f/2 liquid media for cell propagation, and then plated dilutions onto agar plates containing 100 μg mL^{-1} zeocin to obtain single colonies. The genomic DNA from these single colonies was isolated and used as a template for PCR to screen *P. tricornutum ptATS2a* knockdown and *ptATS2b* knockout cell lines. RT-PCR was also conducted for validation of biallelic mutations with large fragment deletion in the obtained mutants.

Complementation of *E. coli plsC*Δ mutant SM2-1

To test whether the *E. coli plsC*Δ mutant (SM2-1) could be complemented by heterologous expression of ptATS2, pQE60 (empty vector) or pQE60 harboring ptATS2a or ptATS2b was transformed into SM2-1 cells. Positive colonies were grown on LB agar plates at 30°C or 42°C to evaluate whether the sensitivity to high temperature of the *E. coli plsC*Δ mutant could be rescued.

Heterologous expression of ptATS2 in the *S. cerevisiae* mutant Y02431

The yeast expression plasmids harboring ptATS2a or ptATS2b or the empty vector (pYES2/CT) were transformed into the yeast mutant Y02431 by the standard lithium acetate procedure (Gietz and Woods, 2002). Transformants were selected by growth on synthetic complete medium (2% glucose [w/v], 0.67% yeast nitrogen base without amino acids) containing appropriate auxotrophic supplements but lacking uracil (SC-Ura). Single colonies were transferred into liquid SC-Ura with 2% glucose and grown at 28°C overnight. To test Lyso-PC sensitivity, each transformant was suspended in sterile distilled water and adjusted to an OD_{600} of 2, 1, 0.5, and 0.1. The resulting 2 μL yeast solution was spotted on an SC-Ura agar plate lacking uracil but supplementing 2% galactose, 1% raffinose and 10 or 30 μg/mL lysoPAF. Cell growth was evaluated after 72 h at 28°C to examine the lyso-PC sensitivity for yeast cell growth.

In vitro acyltransferase activity assays

Lysophospholipid acyltranferase activities were determined by measuring the incorporation of [^{14}C]palmitoyl-CoA or [^{14}C]oleoyl-CoA (acyl donors) into phospholipids in the presence of relevant lysophospholipids (acyl acceptors). Substrate specificity of ptATS2a and ptATS2b towards the other lysophospholipids were performed with *sn*-1-C18:1-lysoPE, *sn*-1-C18:1-lysoPC, *sn*-1-C18:1-lysoPG, or *sn*-1-C18:1-lysoPS, added to the reaction in equimolar concentration, together with two acyl donors:

219 [^{14}C]16:0-CoA or [^{14}C]18:1-CoA.

220 Complementation of *P. tricornutum ATS2* mutants

221 The coding regions of ptATS2a and ptATS2b were amplified by PCR using primer pairs of
222 ptATS2aKO_com-F/R and ptATS2bKO_com-F/R, respectively. Oligonucleotides introduced a 5'
223 *EcoR*I and 3' *Sal*I restriction site for cloning the fragment into pPha-Cp1, a modified pPha-T1 plasmid.
224 In this plasmid, a nourseothricin (NTC) resistance cassette controlled by the FcpD promoter and FcpA
225 terminator (Slattery et al. 2018) is used to replace the zeocin resistance cassette. The *P. tricornutum*
226 *ptATS2a* or *ptATS2b* mutated lines were complemented by microparticle bombardment from
227 logarithmic-phase grown cells with the NTC-resistance plasmid pPha-Cp1 containing the wild-type
228 ptATS2 sequence. Algal transformants were selected on F/2 agar plates supplemented with 50 μg mL^{-1}
229 Zeocin and 200 μg mL^{-1} NTC. Colonies appeared after 3-4 weeks incubation at 22^{o}C with light.

230

231 ## Results

232 **Identification of putative LPAATs in *P. tricornutum***

233 To identify LPAAT enzymes in *P. tricornutum*, the genome of this model diatom
234 (http://protists.ensembl.org/Phaeodactylum_tricornutum/Info/Index/) was searched with Basic Local
235 Alignment Search Tool (BLAST), using a query from a partial sequence containing a region conserved
236 between bacterial, yeast and plant LPAATs. From the results, we examined genes that encoded putative
237 LPAAT containing a phosphate acyltransferase (PlsC) domain, known to catalyze the transfer of a FA
238 to the *sn*-2 position of lysoPA to generate PA in bacteria (Schujman and de Mendoza 2008). We also
239 examined proteins possessing the two conserved motifs (NHX$_4$D and EGTR), which are highly
240 conserved in bacteria, yeast, animal and plant LPAATs (Lewin et al. 1999; Körbes et al. 2016) and
241 have been shown to be the putative catalytic domain and binding domain, respectively. Proteins lacking
242 either of these two motifs were discarded. These searches identified two putative LPAATs that we
243 designated ptATS2a (protein ID: Phatr3_J11916) and ptATS2b (protein ID: Phatr3_J43099). The
244 amino acid sequences of these two diatom LPAATs exhibit only 31%–38% identity to their homologs
245 from bacteria, yeast, plant and green alga. Amino acid sequence alignment revealed that both LPAATs
246 contain highly conserved NHX$_4$D domain, while the Thr residue in the EGTR motif was substituted by
247 Met (EGMR) for ptATS2b (Fig.1a).

248 To test the LPAAT activity of both ptATS2s, each gene was heterologously expressed in *E. coli*

249 *plsC* mutant SM2-1 that is unable to grow at 42°C (Coleman 1990). As shown on plate assay (Fig.1b),
250 all the strains harboring an empty vector (pQE60) or a plasmid containing ptATS2a or ptATS2b
251 exhibited normal cell growth at 30°C; although the *E. coli* mutant strain harboring pQE60 was
252 nonviable at 42°C, heterologous expression of ptATS2a or ptATS2b fully restored cell growth at
253 elevated temperature. To further determine the functionality of both ptATS2s, full-length coding region
254 of ptATS2a or ptATS2b was heterologously expressed in Y02431 (*ale1* or *lca1*Δ), a yeast SLC4
255 (Yor175c)-deficient mutant, under the control of the galactose-inducible *GAL1* promoter. SLC4 acts as
256 the major LPAAT in the yeast *S. cerevisiae*, and it is partially redundant with SLC1 in the synthesis of
257 PA (Benghezal et al. 2007). Deletion of *SLC4* eliminated the microsomal biosynthesis of
258 phosphatidylethanolamine (PE) and phosphatidylcholine (PC), and this mutant has also been shown to
259 be hypersensitive to lyso-platelet-activating factor (lyso-PAF) because reacylation of lysoPAF that was
260 required for cell viability was blocked (Chen et al. 2007). To examine whether heterologously
261 expressed LPAAT can alleviate or eliminate the toxicity of lysoPAF on the Y02431 cells, we tested the
262 growth of yeast transformants containing an empty vector or expressing ptATS2 on plates
263 supplemented with different concentrations of lyso-PAF. As shown in Fig.1c, the mutant Y02431
264 expressing ptATS2a or ptATS2b and harboring the empty pYES2/CT vector grew on plates containing
265 10 μg/ml lyso-PAF. However, when plated with 30 μg/ml lyso-PAF, no growth for the control strain
266 was observed while the mutant Y02431 expressing ptATS2a or ptATS2b was able to grow, confirming
267 lysophospholipid acyltransferase activity of these two *P. tricornutum* LPAATs in the *S. cerevisiae*
268 *lca1*Δ mutant.

269 **Both ptATS2a and ptATS2b encode a lysoPA acyltransferase**

270 The *S. cerevisiae slc4*Δ mutant (Y02431) showed a ~85% decrease in the total LPAAT activity of
271 cellular homogenate relative to wild-type yeast, and the simultaneous deletion of *slc4* and *slc1* is lethal
272 (Benghezal et al. 2007; Riekhof et al. 2007). We thus conducted an *in vitro* enzyme assay using the
273 *slc4*Δ mutant (Y02431) to determine the specificity of both *P. tricornutum* LPAATs towards different
274 lysophospholipids. The acyltransferase activity in microsomes from Y02431 cells, overexpressing
275 ptATS2a or ptATS2b, was first measured using [^{14}C]palmitoyl-CoA and *sn*-1-18:1-LysoPA as
276 substrates. Of tested four colonies, at least three colonies of *S. cerevisiae* Y02431 expressing ptATS2a
277 (Fig.2 a) or ptATS2b (Fig.2 b) had significantly higher LPAAT activity than that in control strain
278 transformed with an empty vector, although there was a low level of endogenous LPAAT activity

encoded by SLC1 in Y02431. Plastidic LPAATs are likely to use acyl-acyl carrier protein (acyl-ACP) in vivo, thus acyl-CoA-substrates might be not sufficient to detect LPAAT activities. Using microsomal fractions of *S. cerevisiae* Y02431 expressing ptATS2a or ptATS2b as enzyme source and [^{14}C]16:0-CoA (Fig.2 c) or [^{14}C]18:1-CoA (Fig.2 d) as acyl donor, we then examined their substrate specificities towards other lysophospholipids. As shown in Fig.2 c,d, when *sn*-1-18:1-lysoPC, lysoPG, lysoPS and lysoPE were used as acyl acceptor, respectively, the microsomal fraction from *S. cerevisiae* Y02431 expressing ptATS2a or ptATS2b exhibited lower (15–80 times) acyltransferase activity than with lysoPA. In the assay containing *sn*-1-18:1-lysoPE and [^{14}C]16:0-CoA as substrates, the microsomal fraction from *S. cerevisiae* Y02431 expressing ptATS2a had two-fold higher acyltransferase activity than that from vector control (Fig.2c).

Both ptATS2a and ptATS2b are localized in the chloroplast

Prediction of transmembrane structures indicated that a transmembrane domain was located near the N-terminus in the region of amino acids 95–123 for ptATS2a, whereas ptATS2b lacks a predicted transmembrane region (Fig.S1). Prediction of putative N-terminal targeting signals revealed that the presequence of ptATS2a contains a plastid-specific bipartite targeting signal (BTS), which is characterized by the presence of an ASAFAP motif typical for proteins translocated across all four membranes surrounding the plastids in diatoms (Apt et al., 2002; Kilian and Kroth, 2005; Gruber et al., 2007). In contrast, only a classical signal peptide (amino acids 1–21) was predicted for ptATS2b. To determine their subcellular localization, the expression of full-length ptATS2 fused with GFP was visualized by confocal microscopy. The expression of ptATS2a-eGFP resulted in more or less concentrated fluorescence signals directly surrounding the plastid autofluorescence, demonstrating a similar fluorescence pattern to TPT4a and TPT4b, two putative triose phosphate translocators (Moog et al. 2015). In contrast, ptATS2b was probably localized in the thylakoid according to the ptATS2b-eGFP fluorescence signals present as spots in the plastid (Fig.3a,b), showing a similar localization to the recently reported malonyl-CoA:ACP transacylase (Huang et al. 2023). To further determine the localization and topologies of both ptATS2s in the plastid, we adapted a self-assembling GFP approach (Cabantous et al. 2005). We fused last beta strand of GFP (GFP_S11), to ptATS2 and co-transformed the diatom with strands 1-10 of GFP (GFP_S1-10) fused to topogenic signals either directing the protein to the inner membrane space (IMS) or the stroma. As shown in Fig.3c, fluorescence signals indicated a self-assembly of GFP in the stroma when co-expressing of

ptATS2a-GFP_S11 with stromal GFP_S1-10 but not in the IMS, indicating that ptATS2a is localized in the inner envelope membrane (IEM) with its C-terminus facing the plastid stroma. Whereas simultaneous expression of ptATS2b-GFP_S11 with the stromal marker fused to GFP_S1-10 resulted in GFP fluorescence, no signal was detectable in combination with the IMS marker (Fig.3d), indicating that ptATS2b is localized in the thylakoid with C-terminus facing the stroma.

Generation of single *ptATS2* knockout mutants using multiplexed CRISPR/Cas9

To characterize the functions of the two plastidial LPAATs in lipid synthesis in *P. tricornutum*, we generated single gene knockout mutants using multiplexed CRISPR/Cas9 method as described by Moosburner et al. (2020). We used Golden Gate cloning to create a set of constructs harboring multiplex gRNA expression cassettes for multiplexed genome editing. For each ptATS2 gene, we created two constructs each carrying three guide RNAs (gRNAs) separately expressed from independent siRNA promoter to simultaneously target endogenous loci in the *P. tricornutum* genome. These constructs carrying multiple gRNA expression cassettes, Cas9 expression cassette and zeocin resistance gene were introduced into *P. tricornutum* by bacterial conjugation. To examine mutation frequencies, the target sites/regions were PCR-amplified and subjected to DNA sequencing. After obtaining single colonies by several rounds of plating dilutions onto agar plates, we then designed a primer pair with one inside the deletion region and the other outside it, and performed PCR to screen positive colonies using genomic DNA as template (Fig.4a,b). The presence of a large fragment deletion within the predicted *PlsC* domain of *ptATS2a* and *ptATS2b* KO mutants was verified by the final DNA sequencing (Fig.4 c-f). These results show that creating deletions of large fragment with two or more gRNAs appears to be an efficient approach to achieve targeted mutagenesis. We chose two or three independent cell lines for each ptATS2 mutants to analyze lipid-associated phenotypes.

Mutations of both *ptATS2* isoforms impair growth and cause strong reduction in TAG accumulation

The *ptATS2a* or *ptATS2b* mutants were first grown in static cultures, and their growth and N consumption of in nutrient-replete medium were very similar to that of wild type (WT) (Fig.5 a,b). Nonpolar lipid content was used as a readout for an impairment of whole glycerolipid homeostasis in *P. tricornutum*. It was evaluated by fluorescence intensity of algal cells stained with Nile Red, and verified by TAG measurement by TLC analyses. After 12 days of cultivation, nonpolar lipid and TAG

contents did not change in *ptATS2a*, whereas they were markedly reduced in *ptATS2b* compared with WT (Fig.5 c,d). When algal cultures were bubbled with air (low CO_2, *c.* 0.04% v/v CO_2), we observed that *ptATS2a* and *ptATS2b* showed a significantly compromised growth compared with WT (Fig.5 e). Nitrate concentrations in the medium in WT, *ptATS2a* and *ptATS2b* were decreased to the lowest level at day 7, 10 and 8 (Fig.5 f), respectively. Nonpolar lipid content and TAG accumulation were significantly reduced after 8 days of cultivation in both *ptATS2a* and *ptATS2b* compared with WT, and *ptATS2a* accumulated less TAGs than *ptATS2b* (Fig.5 g,h). To further examine the effect of *ptATS2* KO on lipid synthesis, we analyzed cell growth and lipid-associated phenotypes of mutants under N deprivation. There is no difference in cell density between the *ptATS2b* mutants and WT, but cell growth of *ptATS2a* was slower than WT after 2 days of N deprivation (Fig.5 i). In addition, *ptATS2a* accumulated less nonpolar lipids and TAGs compared with WT during N deprivation (Fig.5 j,k). Although nonpolar lipid content in *ptATS2b* was reduced at day 2 and 3, it reached WT level at day 4; TAG accumulation in *ptATS2b* did not show marked reduction after 2 days of N deprivation (Fig.5 j,i). These results indicate that both ptATS2s mediate TAG synthesis but they play distinct roles under different conditions. We also measured the photosynthetic activities between WT and the mutants grown in the exponential phase. We observed an impairment of the photosynthetic capacity in the *ptATS2a* mutants as indicated by the significant decrease in PSII efficiency (F_v/F_m) and relative electron transport rate ($rETR_{PSII}$) when compared to WT, while there was no difference between WT and the *ptATS2b* mutants (Fig.S2).

Impacts of the *ptATS2* mutation on glycerolipidomes

Plastid-localized LPAATs could produce metabolic pools of PA feeding dedicated lipid biosynthetic pathways in the plastid and other cellular compartments. To examine the effect of *ptATS2* mutation on lipid composition and the distribution of different molecular species within each lipid class, we analyzed the glycerolipidomes of *P. tricornutum* WT and mutants grown in nutrient-replete medium for 4 d (+N) and in N-depleted medium for 4 d (–N). FA profiles were first analyzed for *P. tricornutum* WT and *ptATS2* mutants, revealing that the major FAs are palmitic acid (16:0), palmitoleic acid (16:1) and EPA at both conditions. KO of *ptATS2b* had little influence on FA composition at both +N and –N conditions whereas the mutation of *ptATS2a* significantly changed the proportion of three major FAs at N-depleted condition. Compared with WT, the main alterations of total FA profile in the *ptATS2a* mutants were observed at N-depleted condition by relative decreases in palmitic and

palmitoleic acids (from 34% in WT to 27% in *ptATS2a* of TFAs, and from 40% in WT to 34% in *ptATS2a* of TFAs, respectively), concomitant with an increase in the proportion of EPA (from 5% in WT to 8% in *ptATS2a* of TFAs) as well as 16:2, 16:3, 18:2 and 18:3 (Fig.S3). Detailed lipidomic analysis revealed that the most noticeable changes of TAGs and molecular composition in each lipid class were observed in the *ptATS2a* mutants. Almost no TAG synthesis was observed when WT and the mutants were grown in nutrient-replete medium for 4 d. However, after algal cells were grown in N-free medium for 4 days, N deprivation led to the accumulation of large amounts of TAGs, which accounted for 56% and 52% of total lipids in WT and *ptATS2b*, respectively, whereas the percentage of TAGs in total lipids in *ptATS2a* was declined to only 27% (Fig.6). In total lipids, SQDG, PG, PI and PC showed a decrease in the *ptATS2a* mutants in N-replete condition when compared to WT supporting a direct impact of the lack of *ptATS2a*. In the *ptATS2a* mutants the level of DAG, which is generated by removal of the *sn*-3 phosphate of PA, was decreased from 0.71% of total lipids in WT to 0.51% ($P<0.01$) in N-replete condition, and from 2.43% of total lipids in WT to 1.24% ($P<0.0001$) in N-deprived condition (Fig.6).

The *ptATS2a* mutants also showed the most significant change of glycerolipid composition. Concerning plastid lipids supposed to be synthesized downstream of LPAATs, MGDG and DGDG in *ptATS2a* had a significant decrease in the levels of molecular species containing 20:5/16:3 and 20:5/16:4 in both N-replete and N-deprived conditions (Fig.7a,b). Moreover, a significant decrease was also observed in *ptATS2b* in the levels of the 20:5/16:3 form representing the most abundant molecular species in MGDG and the 20:5/16:2 form in DGDG in N-replete condition. Compared to WT, two major SQDG species of 14:0/16:0 and 14:0/16:1 had a significant decrease in both *ptATS2a* and *ptATS2b* mutants, and the *ptATS2a* mutants also showed a decrease in the levels of 16:0/24:0 and 16:1/16:0 in N-replete condition (Fig.7c). For PG, two major molecular species of 20:5/16:0 and 20:5/16:1 showed a significant decrease in both conditions (Fig.7d). These changes suggest that inactivation of either *ptATS2a* or *ptATS2b* had a strong influence on molecular composition of all plastid glycerolipids.

PC, PE, and DGTA, likely synthesized in extra-plastidial membranes, also showed several noticeable alterations of molecular profiles in both *ptATS2* mutants. In PC, a significant decrease was observed in the *ptATS2a* mutants in the levels of those molecular species harbouring a 20:5 at the *sn*-1 position and C16/C20/C22 FA at the *sn*-2 position in N-replete condition (Fig.8a, Supporting

information Dataset S1). In the *ptATS2a* mutants, two major PE species of 20:5/20:5 and 20:5/22:6 showed a decrease in both N-replete and N-deprived conditions, whereas the *ptATS2b* mutants only had a slight decrease in the levels of PE 20:5/16:2 and 20:5/18:4 in N-replete condition (Fig.8b). In DGTA, a possible substrate for FA desaturation, the levels of at least 8 molecular species (14:0/16:1, 14:0/16:2, 14:0/20:5, 16:1/18:3, 20:5/16:1, 20:5/22:5, 20:5/22:6 and 22:6/22:6) were significantly decreased in both *ptATS2a* and *ptATS2b* mutants in N-replete condition. In addition, the *ptATS2a* mutants also showed a decrease in the levels of 14:0/20:5, 16:1/18:3, 20:4/20:5, 20:5/20:5, 20:5/22:5 and 20:5/22:6 in N-deprived condition (Fig.8c).

In the DAG pool, the most significant change was a decrease in the 14:0/16:1 form (46%, $P<0.0001$) and disappearance of 14:0/16:0 and 16:0/16:0 (non-detected) in the *ptATS2a* mutants in N-deprived condition (Supporting information Dataset S1). The decrease in 14:0/16:1 species in the DAG pool coincided well with the similar changes of this DAG backbone in MGDG, DGDG and SQDG (Fig.7a-c), which suggests that this DAG moiety of glycolipids might be of the same chloroplast origin. Further quantitative analysis of TAG molecular species revealed that in addition to the significant reduction of TAG content, TAGs from the *ptATS2a* mutants also showed altered molecular composition. Compared with WT, the major changes observed in *ptATS2a* were a decrease in the proportion of TAG species of 14:0/16:1/16:0, 16:0/16:0/16:0, 16:0/16:0/16:1, 16:1/16:1/16:0, and 16:1/16:1/16:1 in both N-replete and N-deprived conditions (Fig.9). In contrast, almost no difference in TAG composition was observed between WT and the *ptATS2b* mutants. These results suggest that the activity of plastidial ptATS2a is involved, indirectly, in regulating TAG content as well as molecular composition of TAGs in *P. tricornutum*. Since plastid and extra-plastidial membrane lipids as well as cytosolic TAG are quantitatively and qualitatively impacted, these phenotypes reflect the importance of plastid LPAAT on the glycerolipid homeostasis at the whole cell level. Taken together, ptATS2a contributes to membrane lipid synthesis and to part of TAG accumulation under N deprivation, while the involvement of ptATS2b in these metabolic pathways, if any, was minor.

Discussion

In this study, we characterized two plastid-localized LPAATs from *P. tricornutum*, which are involved in the synthesis of almost all glycerolipids. Whereas ptATS2a is localized in the plastid IEM, the disruption of *ptATS2a* results in a decrease in the levels of SQDG and PG, which were recently verified to be synthesized in the plastid (Huang et al. 2023). Thus, PA as it is synthesized in the thylakoid by

ptATS2a could possibly be a precursor for SQDG and PG biosynthesis. Unexpectedly, disruption of *ptATS2a* led to an increase rather than a decrease in relative levels of MGDG and DGDG (Fig.6), which were also considered to be synthesized in the plastid. Possible causes are that there are multiple MGDG synthetic pathways present in *P. tricornutum* and the other pathways are upregulated in the *ptATS2a* mutants to compensate for the deficiency in thylakoid MGDG synthesis. Indeed, MGDG synthesis in *P. tricornutum* is catalyzed by three MGD isoforms, which localize to distinct subcellular compartments including thylakoid, periplastidal membrane, ER, and cytosol (our unpublished data), indicating these isoforms are likely non-redundant. These analyses suggest that MGDG, and its derivative DGDG, would not be restricted to thylakoid and IEM, and it is likely that there are multiple routes for MGDG synthesis in diatom cells. Ethanolamine-/choline-phosphotransferase involved in PE and PC synthesis was localized in the cER membrane (Huang et al. 2023), consistent with an occurrence of their syntheses in the cER. The *ptATS2a* mutants grown in N-replete condition showed a decrease in PC, suggesting that PA as it is synthesized at the IEM could possibly provide a direct substrate for PC synthesis. Although how PA/DAG produced by ptATS2a at IEM is transferred to the cER is not known, a PA transporter should be required for this process since PA itself cannot readily traverse the plastid membranes (OEM and PPM). However, we observed an increase in the level of PE in the *ptATS2a* mutants, indicating that PA produced by ptATS2a may not provide a precursor for PE synthesis in the cER and additional PE synthetic pathway possibly exists in *P. tricornutum*. For molecular composition of glycerolipids, our lipidomic analysis highlighted that chloroplast lipids in the *ptATS2a* mutants showed a decrease in the levels of 20:5/16:0 and 20:5/16:1 in PG, in the levels of 20:5/16:3 and 20:5/16:4 in both MGDG and DGDG, and a moderate change in the profile of SQDG, besides a slight decrease in 20:5/16:0 molecular species (Fig.7). In addition, glycerolipids from endomembranes were also impacted, with a decrease of 20:5/(20:4, 20:5 and 22:6) in both PC and PE, and a decrease of 20:4/20:5, 20:5/(20:5, 22:5 and 22:6) in DGTA as well as 14:0/20:5 and 16:1/18:3 in this betaine lipid (Fig.8). Overall, the changes of lipid profiles were therefore consistent with a role of ptATS2a in the *sn*-2 acylation of *sn*-1-lysoPA substrates harboring a 20:4 or a 20:5 at the *sn*-1 position.

By contrast to *ptATS2a*, the impact of *ptATS2b* mutation on glycerolipid composition was less striking, with nearly no impact on PG, a moderate decrease of 20:5/(16:2 and 16:3) in MGDG, of 20:5/(16:1, 16:2 and 16:3) in DGDG, of 20:5/16:0 in SQDG, of 20:5/(20:4, 20:5 and 22:6) in PC and of 20:4/20:5 and 20:5/20:5 in DGTA. For this isoform, the changes of lipid profiles were also consistent

with a role of ptATS2b in the *sn*-2 acylation of a *sn*-1-acyl-glycerol-3-P substrate harboring a 20:4 or a 20:5 at the *sn*-1 position (Fig.10). Based on the molecular species increasing in *ptATS2b*, some of them correspond to molecular species shown to decrease in the *ptATS2a* mutants, such as 20:5/16:0 in DGDG and PG, and 20:4/20:5 and 20:5/20:5 in DGTA in N-replete condition, suggesting that ptATS2a was able, at least partly, to compensate the *ptATS2b* mutation. This compensation mechanism occurring mainly in the plastid was consistent with the absence of impact on the profile of cytosolic TAG.

Our finding that loss-of-function mutations in single *ptATS2* do not completely abolish plastid lipid synthesis and TAG accumulation also implies that there is partially functional redundancy between both ptATS2s and possibly non-plastidial LPAAT isoforms not considered in the present study. Furthermore, our complementation experiment showed that overexpression of ptATS2b in the *ptATS2a* mutants could partly restore algal cell growth and TAG-associated phenotype and *vice versa* (Fig.S4), supporting that disruption of a plastidial ptATS2 gene could, at least in part, be biochemically and physiologically compensated by the other plastid-located ptATS2.

Quantitative RT-PCR analyses showed that transcript levels of both *ptATS2a* and *ptATS2b* increased during N deprivation for 3 d (Fig.S5), indicating an important role of these two plastidial LPAATs in N starvation-induced TAG accumulation. Consistent with their gene expression patterns, disruption of either *ptATS2* resulted in a significant decrease in the amounts of TAGs during N deprivation for 3 d (Fig.5j,k). Interestingly, a greater extent of decrease in the amount of TAGs was seen in *ptATS2a* than that in *ptATS2b* at the stationary phase and under N-deprived condition when compared with WT (Fig.5h,k,i), which is in agreement with the greater extent of increase in the transcript levels of *ptATS2a* compared to that of *ptATS2b*. These results could indicate a greater contribution of ptATS2a than that of ptATS2b to TAG synthesis under N-starved condition. However, previous study showed that overexpression of ptATS2b increased TAG content by 1.8-fold with a significant increase in PUFAs, indicating its potential regulatory role in TAG synthesis (Balamurugan et al. 2017; Wang et al. 2018). In the green alga *Chlamydomonas*, RNAi-mediated suppression of *CrLPAAT2*, which encodes an ER-located chlorophyte-specific LPAAT, caused a reduction of TAG content under N deprivation (Kim et al. 2018). However, the abundance of the major chloroplast membrane glycerolipids including MGDG, DGDG and SQDG was not affected in these *Chlamydomonas* RNAi strains. In contrast to the negligible role of CrLPAAT2 under nutrient-replete conditions in *Chlamydomonas*, our results

demonstrate that both plastidial LPAATs are required for the biosynthesis of storage TAGs and almost all chloroplast and extra-plastidic membrane glycerolipids in nutrient-replete and N-starved conditions. The most striking effect of disruption of *ptATS2* on lipid metabolism was the dramatic decrease in the content of storage TAGs, which could be explained by two possible causes: (1) the reduced supply of plastid-generated PA/DAG that would be further exported to the cytosol as the glycerol backbone for ER-associated TAG synthesis; (2) inhibition of plastidial *de novo* synthesis of FAs. The involvement of a route from chloroplast glycerolipids to TAG could be supported by the abundant presence of chloroplast glycerolipid C16 FAs in TAG and the concomitant reduction of some DAG molecular species in chloroplast galactoglycerolipids and TAGs in the *ptATS2a* mutants. This is also consistent with recent cell biochemistry and proteomic studies of lipid droplets indicating a tight apposition of this cytosolic TAG storage body with the surface of the plastid (Lupette et al. 2019; Leyland et al. 2020).

In conclusion, our data outline the crucial role of two plastidial LPAATs for the biosynthesis of chloroplast thylakoid membrane lipids, extra-plastidic membrane glycerolipids and storage TAGs in *P. tricornutum*. We found that a single plastidial LPAAT enzyme can regulate different downstream glycerolipid pathways under different conditions. The plastid pathway of thylakoid lipid biosynthesis was strongly impaired in either *ptATS2a* or *ptATS2b* mutants. Our data highlight an important role of 20:5-lyso-PA, as a candidate lipid intermediate in the import of 20:5 from the cytosol to the plastid *via* the so-called 'omega pathway'. In addition, the mutants also showed compromised cell growth and strikingly reduced TAG accumulation when algal cultures were bubbled with air. Therefore, it seems likely that both ptATS2s play an essential role in algal cell growth consistent with their involvement in the generation of PA, a central metabolite of primary lipid metabolism and a regulatory molecule in the chloroplast. Future work on the detailed characterization of the plastidial ATS1 and additional ER-located LPAATs will extend our appreciation of the individual contribution of LPAATs to lipid metabolism in this EPA-rich oleaginous diatom.

Figure legends

Fig.1. Identification of two plastid LPAAT acyltransferases in *P. tricornutum*. (**a**) Alignment of *P. tricornutum* plastidic LPAATs and their homologs from plants, green algae, bacteria and yeast. Conserved residues are in white font on a red background and semi-conserved residues are in black font on a yellow background. The amino acid sequences of ptATS2a (Phatr3_J11916) and

519 ptATS2b (Phatr3_J43099) were aligned together with those of characterized LPAATs from
520 *Arabidopsis thaliana* (AtATS2), *Brassica napus* (BnATS2), *Chlamydomonas reinhardtii*
521 (CrLPAAT1), *Escherichia coli* (EcPlsC) and *Saccharomyces cerevisiae* (ScSLC1). (**b**) Expression
522 of either ptATS2a or ptATS2b could rescue the high temperature sensitivity of the *E. coli plsC*
523 mutant, which is deficient in LPAAT. (**c**) Lyso-PAF (lyso-platelet-activating factor) sensitivity
524 test of the *S. cerevisiae lca1*Δ mutant harboring empty vector (pYES2/CT) or expressing either
525 ptATS2a or ptATS2b. Yeast cells were grown in SC-Ura medium supplemented with 2% glucose
526 overnight at 28°C with shaking then transferred to induction medium for 12 h to induce protein
527 expression. Cultures were serial diluted from OD_{600}=2.0 to 0.1. A measure of 2 μl from each
528 dilution was spotted on SC-Ura plates containing 10 or 30 μg/ml lyso-PAF, respectively. The
529 plates were incubated at 28°C for 2 days.
530
531 **Fig.2**. Acyltransferase activity of ptATS2a and ptATS2b towards different lysophospholipids. The
532 enzyme assays were performed with microsomal preparations from the yeast *slc4*Δ mutant
533 expressing the ptATS2 gene or harboring empty vector (pYES2/CT) with different
534 lysophospholipids as acyl acceptor and [^{14}C]16:0-CoA or [^{14}C]18:1-CoA as acyl donor. The
535 LPAAT activities of ptATS2a (**a**) and ptATS2b (**b**) were measured using *sn*-1-C18:1-lysoPA and
536 [^{14}C]16:0-CoA as substrates. The amounts of synthesized [^{14}C]PA during reaction time were
537 treated as the result of LPAAT activity. The lysophospholipid acyltransferase activities of
538 ptATS2a and ptATS2b were tested using [^{14}C]16:0-CoA (**c**) or [^{14}C]18:1-CoA (**d**) as acyl donor.
539 In the enzyme assay, four different lysophospholipids were used as acyl acceptors:
540 *sn*-1-C18:1-lysoPE, *sn*-1-C18:1-lysoPC, *sn*-1-C18:1-lysoPG, or *sn*-1-C18:1-lysoPS.
541 Acyltransferase activities were calculated based on the amounts of synthesized [^{14}C]
542 phospholipids during the reaction time. The representative results of three independent yeast
543 transformants were shown. Mean values and standard deviation are presented (n≥3). Asterisk
544 indicates significant difference from the empty vector control as determined by the Student's *t*-test
545 (*, P<0.05). PE, phosphatidylethanolamine; PC, phosphatidylcholine; PG, phosphatidylglycerol;
546 PS, phosphatidylserine.
547
548 **Fig.3**. Plastid localization of both ptATS2s. (**a**, **b**) ptATS2a and ptATS2b fused to enhanced GFP

were transfected into *P. tricornutum* to determine subcellular localization. (**c**, **d**) the self-assembling split GFP system was adapted in *P. tricornutum*. Both ptATS2a and ptATS2b, fused to GFP_S11 did not show a fluorescence signal when co-expressed with the IMS marker MGD1 fused to GFP_S1-10, whereas a clear GFP signal could be observed upon co-expression with the stromal-targeted AtpC_BTS-GFP_S1-10, respectively. TL, transmitted light; PAF, plastid autofluorescence; GFP, enhanced green fluorescence protein; PAF/GFP, overlay of plastid and GFP fluorescence. PAF is shown in red and GFP fluorescence in green. BTS, bipartite targeting signal; PPC, periplastidal compartment; IMS, intermembrane space; Str, plastid stroma; Scale bar represents 5 or 8 μm.

Fig.4. Genome editing of *ptATS2a* and *ptATS2b* using multiplex CRISPR/Cas9 method led to the generation of fragmental deletions in *P. trcornutum*. Schematic diagrams show the fragmental deletions between two targeted sites of the *ptATS2a* (**a**) and *ptATS2b* (**b**) mutants. A pair of primers was designed to detect the large fragmental deletions induced by multiplex CRISPR/Cas9 in the *ptATS2a* (**c**) and *ptATS2b* (**d**) mutants with PCR using genomic DNAs and total complementary DNA (cDNA) as template. For DNA sequencing, PCR was carried out using primer pairs flanking the predicted target sites, and the PCR products were sequenced directly using internal specific primers. Representative sequences of fragment deletions in the *ptATS2a* (**e**) and *ptATS2b* (**f**) mutants were aligned with that of wild type. The PAM region is shown in blue color letters, and the number at the end shown in red color letters indicates deleted (-) bases between two Cas9 cut sites.

Fig.5. Phenotype analyses of the *ptATS2a* and *ptATS2b* mutants. (**a**) Growth curves of the *ptATS2a* and *ptATS2b* mutants incubated in static cultures for 18 days. Cell densities were determined with a Z2 Coulter Counter. Results are the average of three biological replicates (independent cell lines) with error bars indicating standard deviations (n=3). (**b**) Nitrate concentrations in culture media for the *ptATS2a* and *ptATS2b* mutants incubated in static cultures. (**c**) Nile red fluorescence intensities of *ptATS2a* and *ptATS2b* mutant cells incubated in static cultures for 18 days. Statistical analysis using paired-sample Student's t test was performed by GraphPad Prism (v9.0): **, P<0.01; ***, P<0.001. (**d**) A thin-layer chromatogram of total lipids

579 from wild type, the *ptATS2a* and *ptATS2b* mutants incubated in static cultures for 13 d, 14 d, and
580 15 d. Each lipid sample was extracted from ~5×10^7 cells. TAGs were visualized with 0.01% (w/v)
581 primuline reagent. (**e**) Growth curves of the *ptATS2a* and *ptATS2b* mutants under air bubbling
582 condition for 12 days. Data are the average of three biological replicates (independent cell lines)
583 with error bars indicating standard deviations (n=3). (**f**) Nitrate concentrations in culture media for
584 the *ptATS2a* and *ptATS2b* mutant cultures bubbled with filtered air. (**g**) Nile red fluorescence
585 intensities of the *ptATS2a* and *ptATS2b* mutant cultures bubbled with filtered air for 6-12 days.
586 Statistical analysis using paired-sample Student's *t* test was performed by GraphPad Prism (v9.0):
587 **, P<0.01; ***, P<0.001. (**h**) TLC of total lipids from wild type and the *ptATS2a* and *ptATS2b*
588 mutants grown in air-bubbling condition for 8 d, 9 d and 10 d . Each lipid sample was extracted
589 from ~5×10^7 cells. (**i**) Growth curves of the *ptATS2a* and *ptATS2b* mutants under nitrogen
590 deprivation for 4 days. Data are the average of three biological replicates (independent cell lines)
591 with error bars indicating standard deviations (n=3). (**j**) Nile red fluorescence intensities of algal
592 cells of the *ptATS2a* and *ptATS2b* mutants grown under nitrogen deprivation for 4 days. Statistical
593 analysis using paired-sample Student's *t* test was performed by GraphPad Prism (v9.0): **,
594 P<0.01; ***, P<0.001; ****, P<0.0001. A TLC of total lipids from wild type and the *ptATS2a* (**k**)
595 and *ptATS2b* (**l**) mutants grown under nitrogen deprivation for 4 d verified the change of TAG
596 accumulation. Each lipid sample was extracted from ~5×10^7 cells.
597
598 **Fig.6**. Quantification of different molecular species of TAG in the *ptATS2a* knockdown (KD) and
599 *ptATS2b* knockout mutants in three biological replicates using LC-MS. Each TAG species is
600 shown as N:M, where N is the number of carbon atoms in acyl-chains and M is the number of
601 C=C double bonds. The size of the corresponding circle followed by each TAG species indicates
602 the average percentage of total TAG represented by wild type. A heat map shows the percentage
603 abundance of each species in each biological replicates relative to the average percentage
604 abundance of that species in wild type.
605
606 **Fig.7**. Impact of ptATS2a knock down (KD) and ptATS2b knockout (KO) on the relative amounts
607 (mol%) of molecular species in plastidial glycolipids including (**a**)
608 monogalactosyldiacylglycerol/MGDG, (**b**) digalactosyldiacylglycerol/DGDG and (**c**)

609 sulfoquinovosyldiacylglycerol/SQDG. *P. tricornutum* wild type and mutant cells were harvested
610 at day 8 and day 10 from algal cultures bubbled with filtered air. Data are means ± SD (*n*=3) and
611 asterisks indicate significant difference from wild type as determined by the Student's *t*-test (*,
612 *P*<0.05; **, *P*<0.01; ***, *P*<0.001; ****, *P*<0.0001).
613
614 **Fig.8**. Impact of ptATS2a knockdown (KD) and ptATS2b knockout (KO) on the relative amounts
615 (mol%) of molecular species in (**a**) phosphatidylcholine (PC) and (**b**) the betaine glycerolipid
616 diacylglyceryl-hydroxymethyl-*N*,*N*,*N*-trimethyl-β-alanine (DGTA). *P. tricornutum* wild type and
617 mutant cells were harvested at day 8 and day 10 from algal cultures bubbled with filtered air. Data
618 are means ± SD (*n*=3) and asterisks indicate significant difference from wild type as determined
619 by the Student's *t*-test (*, *P*<0.05; **, *P*<0.01; ***, *P*<0.001; ****, *P*<0.0001).
620
621 **Fig.9**. Impact of ptATS2a knock down (KD) and ptATS2b knockout (KO) on the relative amounts
622 (mol%) of molecular species in plastidial glycolipids from *P. tricornutum* wild type and the
623 mutants grown under nitrogen deprivation for 4 days. The glycolipids analyzed include (**a**)
624 monogalactosyldiacylglycerol/MGDG, (**b**) digalactosyldiacylglycerol/DGDG, (**c**)
625 sulfoquinovosyldiacylglycerol/SQDG, and (**d**) phosphatidylglycerol/PG. Data are means ± SD
626 (*n*=3) and asterisks indicate significant difference from wild type as determined by the Student's
627 *t*-test (*, *P*<0.05; **, *P*<0.01; ***, *P*<0.001; ****, *P*<0.0001).
628
629 **Fig.10**. A proposed model depicting the role of ptATS2a and ptATS2b in the biosynthesis of
630 chloroplast membrane lipids and TAGs in the diatom *P. tricornutum*. This model summarized the
631 major steps of the generation of PA/DAG in the plastid and the ER, providing precursors of
632 glycerol backbone for the synthesis of chloroplast membrane lipids and storage TAGs,
633 respectively. The plastid pathway begins with acylation of G3P with acyl-ACP by ATS1, leading
634 to the generation of lysoPA. Further acylation of the *sn*-2 position of lysoPA to form PA is
635 catalyzed by the chloroplast-localized ATS2. PA is dephosphorylated to form DAG, which is used
636 for biosynthesis of chloroplast membrane glycolipids including MGDG, DGDG and SQDG. The
637 protein localization and alteration of glycerolipidomic profiles of the *ptATS2a* and *ptATS2b*
638 mutants support their role in the chloroplast in the *sn*-2 acylation of

sn-1-acyl-glycerol-3-phosphate substrates harboring a 20:5 at the *sn*-1 position. The Kennedy pathway for TAG assembly is also shown to illustrate the contrasting reaction of storage TAG accumulation under nitrogen starvation. In this pathway, ER-located lysophosphatidic acid acyltransferase (LPAAT) catalyzes the conversion of lysoPA to PA, which is then dephosphorylated by phosphatidic acid phosphatase (PAP) to form DAG. As an immediate precursor, DAG is used for TAG production under nitrogen limitation through the acyl-CoA-dependent acylation of the *sn*-3 position by diacylglycerol acyltransferase. GPAT, glycerol-3-phosphate acyltransferase; LPAAT, lysophophatidic acid acyltransferase; DGAT, diacylglycerol acyltranferase; LACS, long-chain acyl-CoA synthetase; G3P, lysoPA, lysophosphatidic acid; PA, phosphatidic acid; DAG, diacylglycerol; MGDG, monogalactosyldiacylglycerol; DGDG, digalactosyldiacylglycerol.

Acknowledgements

We would like to thank Prof. Xudong Xu (Institute of Hydrobiology, Chinese Academy of Sciences, China) for providing the *E. coli plsC* mutant SM2-1. We also thank Fang Zhou (Analysis and Testing Center of Institute of Hydrobiology, Chinese Academy of Sciences) for technical assistance in fluorescence microscopy analysis. This work was supported by the grant from the National Natural Science Foundation of China (31961133008 to YG) and in part by the International Partnership Program of Chinese Academy of Sciences (Grant No. 075GJHZ2022014MI to HH). A. Amato, JJ and EM were also supported by Agence Nationale de la Recherche (ANR-10-LABEX-04 GRAL Labex, Grenoble Alliance for Integrated Structural Cell Biology; ANR-11-BTBR-0008 Océanomics; IDEX UGA CDP Glyco@Alps; Institut Carnot 3BCAR). The Polish group was financially supported by the National Science Center (NCN, Poland; No. UMO-2018/30/Q/NZ3/00497 to AB). This study was additionally funded by grants from the United States Department of Energy Genomics Science program, the US National Science Foundation, NSF-MCB-1818390, and the Gordon and Betty Moore Foundation GBMF3828 (to AEA).

Authors' contributions

LY, AP, KJG, FR, XH and HJ performed experiments. JJ, EM, AB and HH analyzed the data. A. Allen contributed to the multiplexed CRISPR/Cas9 vectors and methods. YG and A. Amato planed and designed the research. YG wrote the manuscript and JJ, EM and A. Amato revised the manuscript.

Data availability

The data that support the findings of this study are available in the supplementary material of this article.

References

Abida H, Dolch LJ, Mei C, Villanova V, Conte M, Block MA, Finazzi G, Bastien O, Tirichine L, Bowler C, Rébeillé F, Petroutsos D, Jouhet J, Maréchal E. 2015. Membrane glycerolipid remodeling triggered by nitrogen and phosphorus starvation in *Phaeodactylum tricornutum*. *Plant Physiology*, 167: 118-136.

Alvarez HM, Steinbuchel A. 2002. Triacylglycerols in prokaryotic microorganisms. *Applied Microbiology and Biotechnology*, 60: 367-376.

Andrès C, Agne B, Kessler F. 2010. The TOC complex: preprotein gateway to the chloroplast. *Biochimica et Biophysica Acta*, 1803: 715-723.

Apt KE, Zaslavkaia L, Lippmeier JC, Lang M, Kilian O, Wetherbee R, Grossman AR, Kroth PG. 2002. In vivo characterization of diatom multipartite plastid targeting signals. *J Cell Sci*, 115: 4061-4069.

Awai K, Xu C, Lu B, Benning C. 2006. Lipid trafficking between the endoplasmic reticulum and the chloroplast. *Biochem Soc Trans*, 34(Pt 3):395-8.

Balamurugan S, Wang X, Wang HL, An CJ, Li H, Li DW, Yang WD, Liu JS, Li HY. 2017. Occurrence of plastidial triacylglycerol synthesis and the potential regulatory role of AGPAT in the model diatom *Phaeodactylum tricornutum*. *Biotechnology for Biofuels*, 10:97. doi: 10.1186/s13068-017-0786-0.

Benghezal M, Roubaty C, Veepuri V, Knudsen J, Conzelmann A. 2007. SLC1 and SLC4 encode partially redundant acyl-coenzyme A 1-acylglycerol-3-phosphate O-acyltransferases of budding yeast. *The Journal of Biological Chemistry*, 282: 30845-30855.

Benning C. 2008. A role for lipid trafficking in chloroplast biogenesis. *Progress in Lipid Research*,

47: 381-389.

Butler T, Kapoore RV, Vaidyanathan S. 2020. *Phaeodactylum tricornutum*: A Diatom Cell Factory. *Trends in Biotechnology*, 38: 606-622.

Cabantous S, Terwilliger TC, Waldo GS. 2005. Protein tagging and detection with engineered self-assembling fragments of green fluorescent protein. *Nature Biotechnology*, 23:102–107.

Chen Q, Kazachkov M, Zheng Z, Zou J. 2007. The yeast acylglycerol acyltransferase LCA1 is a key component of Lands cycle for phosphatidylcholine turnover. *FEBS Letters*, 581: 5511-5516.

Coleman J. 1990. Characterization of *Escherichia coli* cells deficient in 1-acyl-sn-glycerol-3-phosphate acyltransferase activity. *The Journal of Biological Chemistry*, 265: 17215-17221.

Collos Y, Mornet F, Sciandra A, Waser N, Larson A, Harrison PJ. 1999. An optical method for the rapid measurement of micromolar concentrations of nitrate in marine phytoplankton cultures. *Journal of Applied Phycology*, 11: 179-184.

Cullinane M, Baysse C, Morrissey JP, O'Gara F. 2005. Identification of two lysophosphatidic acid acyltransferase genes with overlapping function in *Pseudomonas fluorescens*. *Microbiology* (Reading). 151:3071-3080.

Dolch LJ, Marechal E. 2015. Inventory of fatty acid desaturases in the pennate diatom *Phaeodactylum tricornutum*. *Marine Drugs*, 13:1317-1339.

Dolch LJ, Rak C, Perin G, Tourcier G, Broughton R, Leterrier M, Morosinotto T, Tellier F, Faure JD, Falconet D, Jouhet J, Sayanova O, Beaudoin F, Marechal E. 2017. A palmitic acid elongase affects eicosapentaenoic acid and plastidial monogalactosyldiacylglycerol levels in *Nannochloropsis*. *Plant Physiology*, 173:742-759.

Frentzen M, Heinz E, McKeon TA, Stumpf PK. 1983. Specificities and selectivities of glycerol-3-phosphate acyltransferase and monoacylglycerol-3-phosphate acyltransferase from pea and spinach chloroplasts. *European Journal of Biochemistry*, 129: 629-636.

Gietz RD, Woods RA. Transformation of yeast by lithium acetate/single-stranded carrier DNA/polyethylene glycol method. 2002. *Methods in Enzymology*, 350:87-96.

Grosche C, Hempel F, Bolte K, Zauner S, Maier UG. 2014. The periplastidal compartment: a naturally minimized eukaryotic cytoplasm. *Curr Opin Microbiol*, 22:88-93..

Gruber A, Vugrinec S, Hempel F, Gould SB, Maier UG, Kroth PG. 2007. Protein targeting into complex diatom plastids: functional characterisation of a specific targeting motif. *Plant Molecular Biology*, 64(5):519-30.

Guillard, RRL. 1975. Culture of phytoplankton for feeding marine invertebrates. In Culture of Marine Invertebrate Animals; Smith W, Chanley M, eds. Springer: New York, 29-60.

Haslam RP, Hamilton ML, Economou CK, Smith R, Hassall KL, Napier JA, Sayanova O. Overexpression of an endogenous type 2 diacylglycerol acyltransferase in the marine diatom *Phaeodactylum tricornutum* enhances lipid production and omega-3 long-chain polyunsaturated fatty acid content. *Biotechnology for Biofuels*, 13:87. doi: 10.1186/s13068-020-01726-8.

Heinz E, Roughan G. 1983. Similarities and differences in lipid metabolism of chloroplasts isolated from 18:3 and 16:3 plants. *Plant Physiology*, 72: 273-279.

Hempel F, Bullmann L, Lau J, Zauner S, Maier UG. 2009. ERAD-derived preprotein transport across the second outermost plastid membrane of diatoms. *Molecular Biology and Evolution*, 26: 1781-1790.

Hu Q, Sommerfeld M, Jarvis E, Ghirardi M, Posewitz M, Seibert M, Darzins A. 2008. Microalgal triacylglycerols as feedstocks for biofuel production: perspectives and advances. *The Plant Journal*, 54: 621-639.

Huang T, Pan Y, Maréchal E, Hu H. 2023. Proteomes reveal the lipid metabolic network in the complex plastid of *Phaeodactylum tricornutum*. *The Plant Journal*, doi: 10.1111/tpj.16477

Jouhet J, Lupette J, Clerc O, Magneschi L, Bedhomme M, Collin S, Roy S, Maréchal E, Rébeillé F. 2017. LC-MS/MS versus TLC plus GC methods: Consistency of glycerolipid and fatty acid profiles in microalgae and higher plant cells and effect of a nitrogen starvation. *Plos ONE*, 12: e0182423.

Karas BJ, Diner RE, Lefebvre SC, McQuaid J, Phillips AP, Noddings C, Brunson JK, Valas RE, Deerinck TJ, Jablanovic J. 2015. Designer diatom episomes delivered by bacterial conjugation. *Nature Communications*, 6: 6925.

Karki N, Johnson BS, Bates PD. 2019. Metabolically distinct pools of phosphatidylcholine are involved in trafficking of fatty acids out of and into the chloroplast for membrane production. *Plant Cell*, 31(11):2768-2788.

757 Kilian O, Kroth PG. 2005. Identification and characterization of a new conserved motif within the
758 presequence of proteins targeted into complex diatom plastids. *Plant J*, 41:175-183.
759 Kim HU, Huang AH. 2004. Plastid lysophosphatidylacyltransferase is essential for embryo
760 development in *Arabidopsis*. *Plant Physiology*, 134: 1206-1216.
761 Kim Y, Terng EL, Riekhof WR, Cahoon EB, Cerutti H. 2018. *Endoplasmic reticulum*
762 acyltransferase with prokaryotic substrate preference contributes to triacylglycerol assembly
763 in *Chlamydomonas*. *Proc Natl Acad Sci U S A*,115(7):1652-1657.
764 Körbes AP, Kulcheski FR, Margis R, Margis-Pinheiro M, Turchetto-Zolet AC. 2016. Molecular
765 evolution of the lysophosphatidic acid acyltransferase (LPAAT) gene family. *Molecular*
766 *Phylogenetics and Evolution*, 96: 55-69.
767 Kovcás-Bogdán E, Soll J, BÖlter B. 2010. Protein import into chloroplasts: the Tic complex and
768 its regulation. *Biochimica et Biophysica Acta*, 1803: 740-747.
769 Kunst L, Browse J, Somerville C. 1988. Altered regulation of lipid biosynthesis in a mutant of
770 Arabidopsis deficient in chloroplast glycerol-3-phosphate acyltransferase activity. *Proceedings*
771 *of the National Academy of Sciences of the United States of America*, 85: 4143-4147.
772 Lenka SK, Carbonaro N, Park R, Miller SM, Thorpe I, Li Y. 2016. Current advances in molecular,
773 biochemical, and computational modeling analysis of microalgal triacylglycerol biosynthesis.
774 *Biotechnology Advances*, 34: 1046-1063.
775 Lewin TM, Wang P, Coleman RA. 1999. Analysis of amino acid motifs diagnostic for the
776 *sn*-glycerol-3-phosphate acyltransferase reaction. *Biochemistry*, 38: 5764-5771.
777 Leyland B, Zarka A, Didi-Cohen S, Boussiba S, Khozin-Goldberg I. 2020. High resolution
778 proteome of lipid droplets isolated from the pennate diatom *Phaeodactylum tricornutum*
779 (Bacillariophyceae) strain pt4 provides mechanistic insights into complex intracellular
780 coordination during nitrogen deprivation. *Journal of Phycology*, 56:1642-1663
781 Lu B, Benning C. 2009. A 25-amino acid sequence of the *Arabidopsis* TGD2 protein is sufficient
782 for specific binding of phosphatidic acid. *The Journal of Biological Chemistry*, 284:
783 17420-17427.
784 Lupette J, Jaussaud A, Seddiki K, Morabito C, Brugière S, Schaller H, Kuntz M, Putaux JL,
785 Jouneau PH, Rébeillé F, Falconet D, Couté Y, Jouhet J, Tardif M, Salvaing J, Maréchal E. 2019.
786 The architecture of lipid droplets in the diatom *Phaeodactylum tricornutum*. *Algal Research*,

787 38:101415
788 Merchant SS, Kropat J, Liu B, Shaw J, Warakanont J. 2012. TAG, you're it! Chlamydomonas as a
789 reference organism for understanding algal triacylglycerol accumulation. *Current Opinion in*
790 *Biotechnology*, 23: 352-363.
791 Miège C, Maréchal É. 1999. 1,2-*sn*-Diacylglycerol in plant cells: Product, substrate and regulator.
792 *Plant Physiol Biochem*, 37(11):795-808.
793 Moosburner MA, Gholami P, McCarthy JK, Tan M, Bielinski VA, Allen AE. 2020. Multiplexed
794 Knockouts in the Model Diatom *Phaeodactylum* by Episomal Delivery of a Selectable Cas9.
795 *Frontiers in Microbiology*, 11: 5.
796 Niu YF, Wang X, Hu DX, Balamurugan S, Li DW, Yang WD, Liu JS, Li HY. 2016. Molecular
797 characterization of a glycerol-3-phosphate acyltransferase reveals key features essential for
798 triacylglycerol production in *Phaeodactylum tricornutum*. *Biotechnology for Biofuels*, 9:60. doi:
799 10.1186/s13068-016-0478-1.
800 Riekhof WR, Wu J, Jones JL, Voelker DR. 2007. Identification and characterization of the major
801 lysophosphatidylethanolamine acyltransferase in *Saccharomyces cerevisiae*. *The Journal of*
802 *Biological Chemistry*, 282: 28344-28352.
803 Okazaki K, Sato N, Tsuji N, Tsuzuki M, Nishida I. 2006. The significance of C16 fatty acids in
804 the *sn*-2 positions of glycerolipids in the photosynthetic growth of *Synechocystis* sp. PCC6803.
805 *Plant Physiol*, 141(2):546-556.
806 Petroutsos D, Amiar S, Abida H, Dolch LJ, Bastien O, Rebeille F, Jouhet J, Falconet D, Block
807 MA, McFadden GI, Bowler C, Botte C, Marechal E. 2014. Evolution of galactoglycerolipid
808 biosynthetic pathways--from cyanobacteria to primary plastids and from primary to secondary
809 plastids. *Progress in Lipid Research*, 54: 68-85.
810 Roughan PG, Slack CR. 1982. Cellular organization of glycerolipid metabolism. *Annual Review of*
811 *Plant Physiology*, 33: 97-132.
812 Schujman GE, de Mendoza D.2008. Regulation of type II fatty acid synthase in Gram-positive
813 bacteria. *Current Opinion in Microbiology*, 11: 148-152.
814 Scott SA, Davey MP, Dennis JS, Horst I, Howe CJ, Lea-Smith DJ, Smith AG. 2010. Biodiesel
815 from algae: challenges and prospects. *Current Opinion in Biotechnology*, 21: 277-286.
816 Slack CR, Roughan PG, Balasingham N. 1977. Labelling studies in vivo on the metabolism of the

817 acyl and glycerol moieties of the glycerolipids in the developing maize leaf. *The Biochemical*
818 *Journal*, 162: 289-296.
819 Slattery SS, Diamond A, Wang H, Therrien JA, Lant JT, Jazey T, Lee K, Klassen Z,
820 Desgagné-Penix I, Karas BJ, Edgell DR. 2018. An expanded plasmid-based genetic toolbox
821 enables Cas9 genome editing and stable maintenance of synthetic pathways in *Phaeodactylum*
822 *tricornutum*. *ACS Synthetic Biology*, 7: 328-338.
823 Wang X, Dong HP, Wei W, Balamurugan S, Yang WD, Liu JS, Li HY. 2018. Dual expression of
824 plastidial GPAT1 and LPAT1 regulates triacylglycerol production and the fatty acid profile in
825 *Phaeodactylum tricornutum*. *Biotechnology for Biofuels*, 11:318. doi:
826 10.1186/s13068-018-1317-3.
827 Wang X, Liu SF, Li RY, Yang WD, Liu JS, Lin CSK, Balamurugan S, Li HY. 2020. TAG
828 pathway engineering via GPAT2 concurrently potentiates abiotic stress tolerance and
829 oleaginicity in *Phaeodactylum tricornutum*. *Biotechnology for Biofuels*, 13:160. doi:
830 10.1186/s13068-020-01799-5.
831 Xin Y, Shen C, She Y, Chen H, Wang C, Wei L, Yoon K, Han D, Hu Q, Xu J. 2019. Biosynthesis
832 of Triacylglycerol Molecules with a Tailored PUFA Profile in Industrial Microalgae.
833 *Molecular Plant*, 12: 474-488.
834 Xu C, Cornish AJ, Froehlich JE, Benning C. 2006. Phosphatidylglycerol biosynthesis in
835 chloroplasts of *Arabidopsis* mutants deficient in acyl-ACP glycerol-3-phosphate
836 acyltransferase. *The Plant Journal*, 47: 296-309.
837 Xu C, Fan J, Froehlich JE, Awai K, Benning C. 2005. Mutation of the TGD1 chloroplast envelope
838 protein affects phosphatidate metabolism in *Arabidopsis*. *The Plant Cell*, 17: 3094-3110.
839 Xu C, Shanklin J. 2016. Triacylglycerol Metabolism, Function, and Accumulation in Plant
840 Vegetative Tissues. *Annual Review of Plant Biology*, 67: 179-206.
841 Yamaoka Y, Achard D, Jang S, Legéret B, Kamisuki S, Ko D, Schulz-Raffelt M, Kim Y, Song
842 WY, Nishida I, Li-Beisson Y, Lee Y. 2016. Identification of a *Chlamydomonas* plastidial
843 2-lysophosphatidic acid acyltransferase and its use to engineer microalgae with increased oil
844 content. *Plant Biotechnology Journal*, 14: 2158-2167.
845 You L, Jouhet J, Maréchal E, Amato A, Hao X, Zhang D, Banaś A, Gong Y. 2023.
846 Acyl-CoA:lysophosphatidylcholine acyltransferase from the unicellular diatom *Phaeodactylum*

tricornutum (PtLPCAT1) is involved in triacylglycerol and galactoglycerolipid synthesis and enhances eicosapentaenoic acid accumulation in recombinant oleaginous yeast. *Plant Biotechnology Journal*, 21(2):238-240.

Zaslavskaia LA, Lippmeier JC, Kroth PG, Grossman AR, Apt KE. 2000. Transformation of the diatom *Phaeodactylum tricornutum* (Bacillariophyceae) with a variety of selectable marker and reporter genes. *Journal of Phycology*, 36: 379-386.

Figure1

(a)

```
AtATS2      NLPSSDTPAVYVSNHQSFLDIYTLLSLGKS..FKFISKTGIFVIPIIGWAMSMMGVVPLKRMD
BnATS2      NLPSSDTPCVYVSNHQSFLDIYTLLSLGQS..YKFISKTGIFVIPVIGWAMSMMGVVPLKRMD
CrLPAAT1    NLPPPDKPVVYVANHQSFLDIYSLFHLQRP..FKFISKTSNFLIPIIGWSMFLTGHVMINRVD
ptATS2a     SFYKEGRPAMFVANHNSWMDIPYLGSTIGWRNYKIIAKKELSKVPALGKAIYLGGHVMVDRTD
ptATS2b     RLKSSQGPCLYVANHASWLDIPVICTVLDP.VFKFIAKGELRKVPCIGQQLEGGNHILIDREN
EcPlsC       TDAESYGNAIYIANHQNNYDMVTASNIVQP.PTVTVGKKSLLWIPFFGQLYWLTGNLLIDRNN
ScSLC1      ENLAKKP.YIMIANHQSTLDIFMLGRIFPP.GCTVTAKKSLKYVPFLGWFMALSGTYFLDRSK

AtATS2      PRSQVDCLKRCMELLKKG.ASVFFFPEGTRSKDG..RLGSFKKGAFTVAAKTGVAVVPITLMG
BnATS2      PRSQVDCLKRCMELVKKG.ASVFFFPEGTRSKDG..RLGPFKKGAFTIAAKTGVPVVPITLMG
CrLPAAT1    RRSQLKCLQQCRDLLAEG.APVLFFPEGTRSLDC..KMAGFKKGAFSVAAKAGVEVVPITLLG
ptATS2a     RKSQLKTLKTGIQYLKDG.VHLCTFPEGTRSRTG..KVLPFKNGAFKMAYKAGAPIIPLSIVG
ptATS2b     RRSQLRTFKDGIGWLKKG.VPIMAFPEGMRSRDG..KLMDFKGGLFSMAVKTQVPIVPITISH
EcPlsC      RTKAHGTIAEVVNHFKKRRISIWMFPEGTRSRG..RGLLPFKTGAFHAAIAAGVPIIPVCVST
ScSLC1      RQEAIDTLNKGLENVKKNKRALWVFPEGTRSYTSELTMLPFKKGAFHLAQQGKIPIVPVVVSN
```

(b)

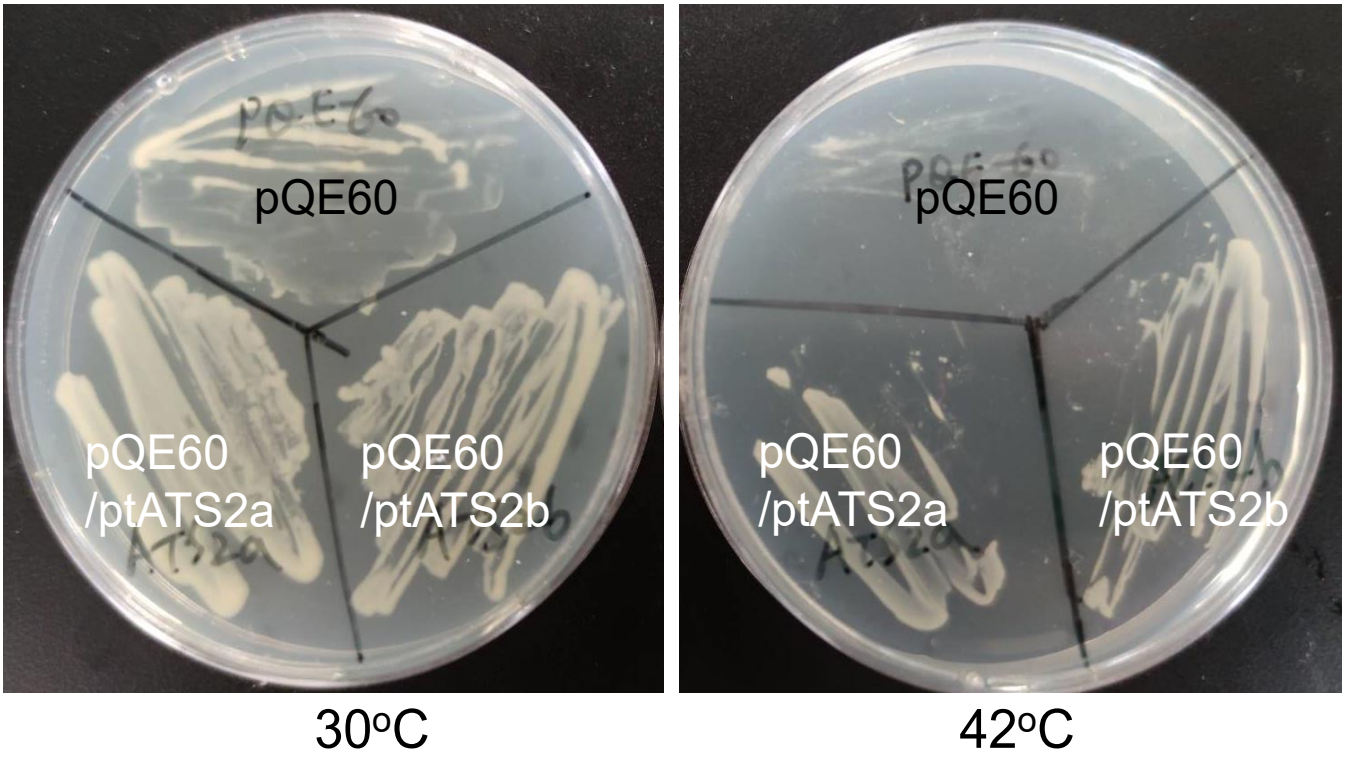

(c)

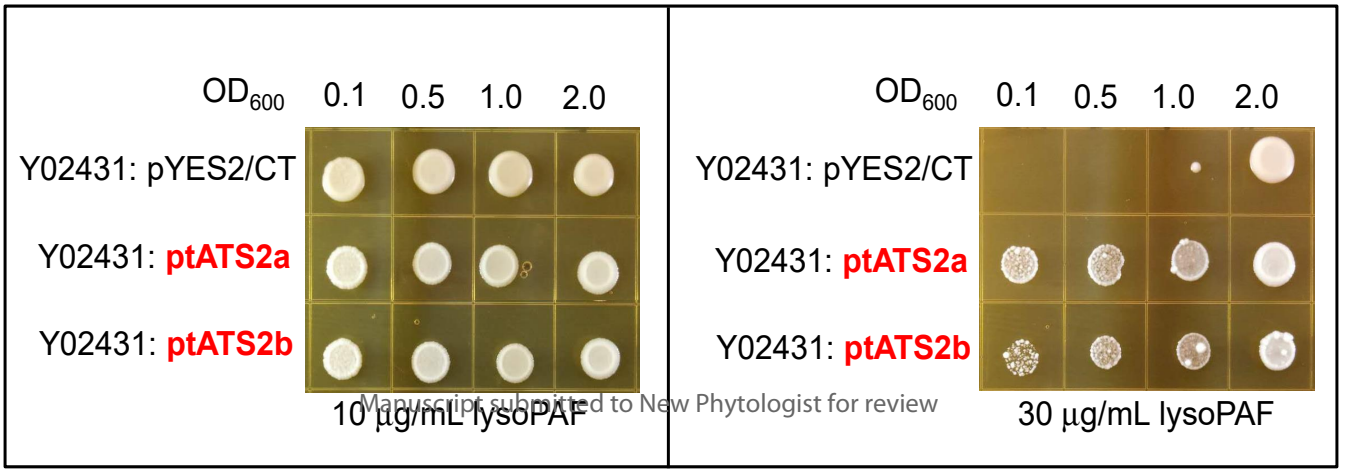

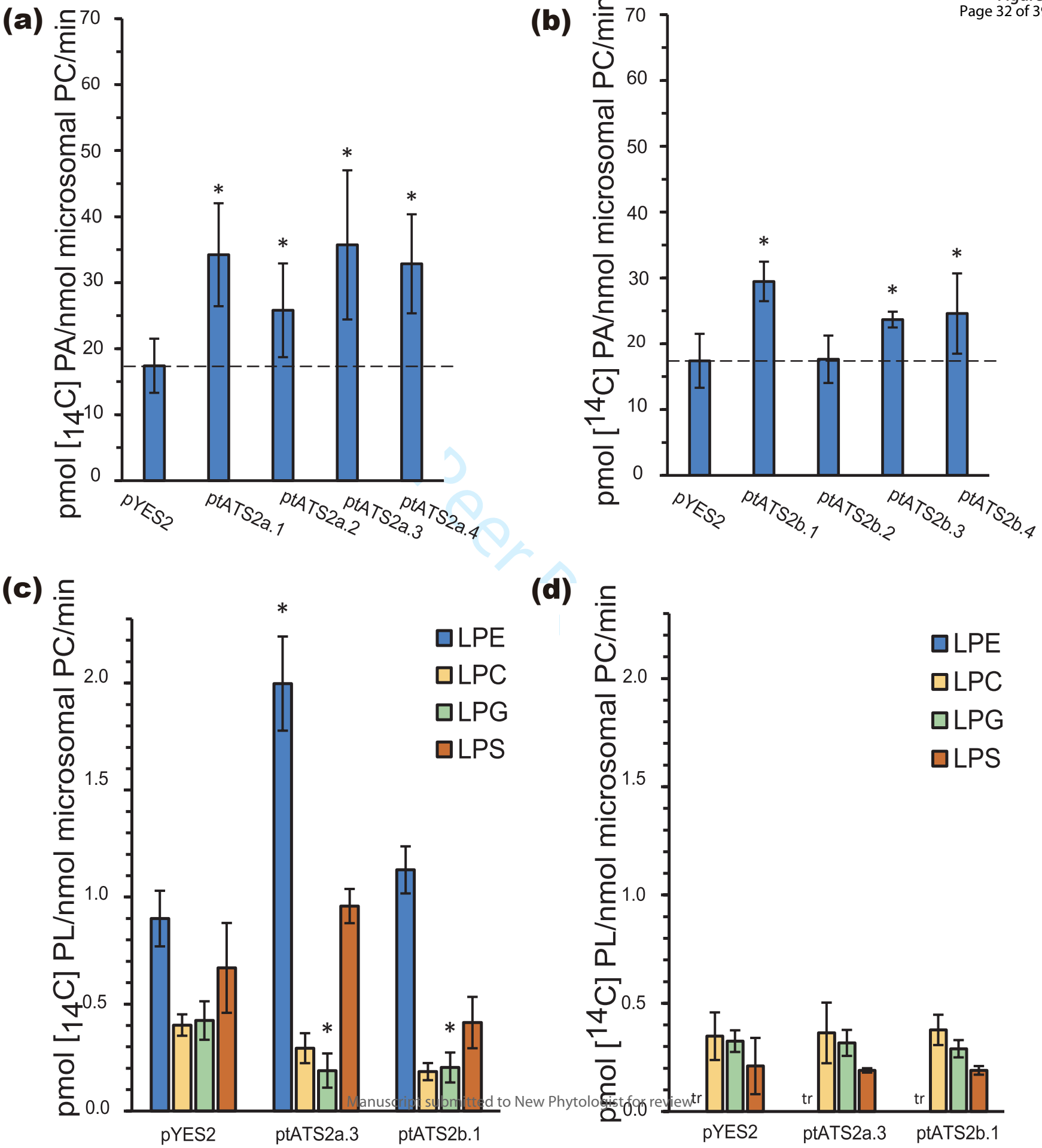

Figure3

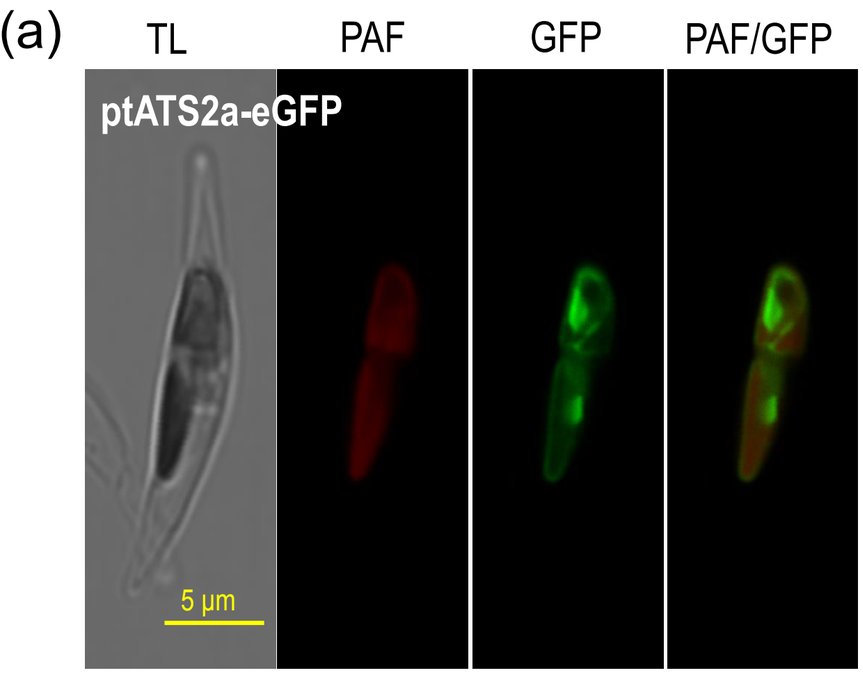
(a)
TL
PAF
GFP
PAF/GFP
ptATS2a-eGFP
5 µm

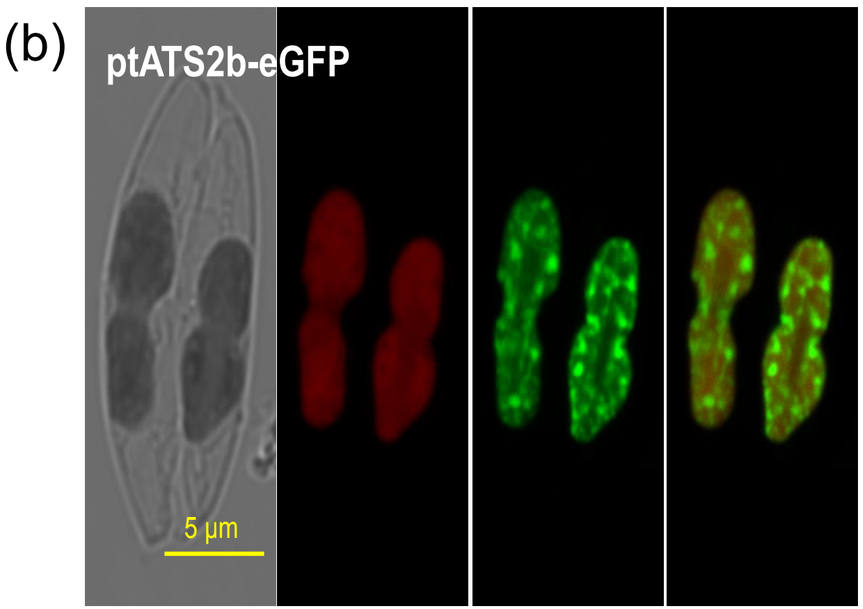
(b)
ptATS2b-eGFP
5 µm

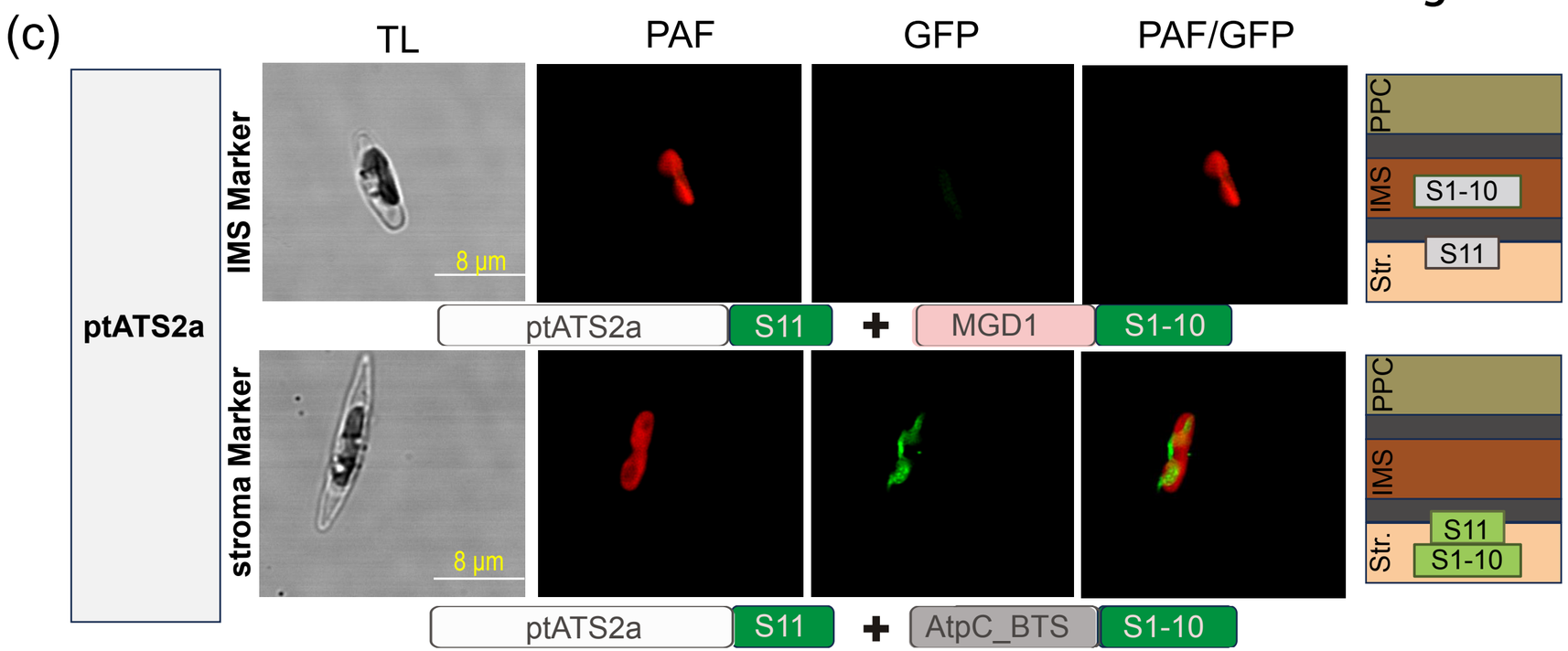
(c)
TL
PAF
GFP
PAF/GFP
ptATS2a
IMS Marker
8 µm
ptATS2a
S11
+
MGD1
S1-10
PPC
IMS
S1-10
Str.
S11
stroma Marker
8 µm
ptATS2a
S11
+
AtpC_BTS
S1-10
PPC
IMS
Str.
S11
S1-10

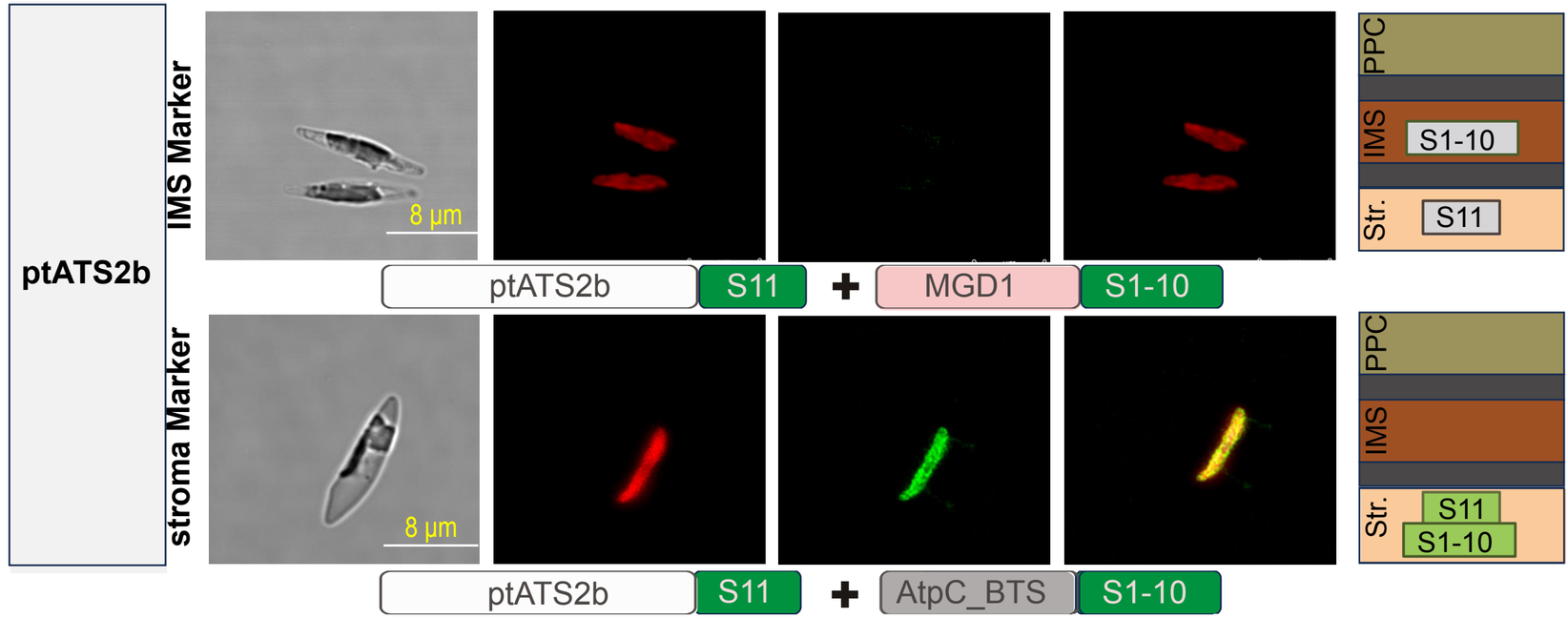
(d)
ptATS2b
IMS Marker
8 µm
ptATS2b
S11
+
MGD1
S1-10
PPC
IMS
S1-10
Str.
S11
stroma Marker
8 µm
ptATS2b
S11
+
AtpC_BTS
S1-10
PPC
IMS
Str.
S11
S1-10

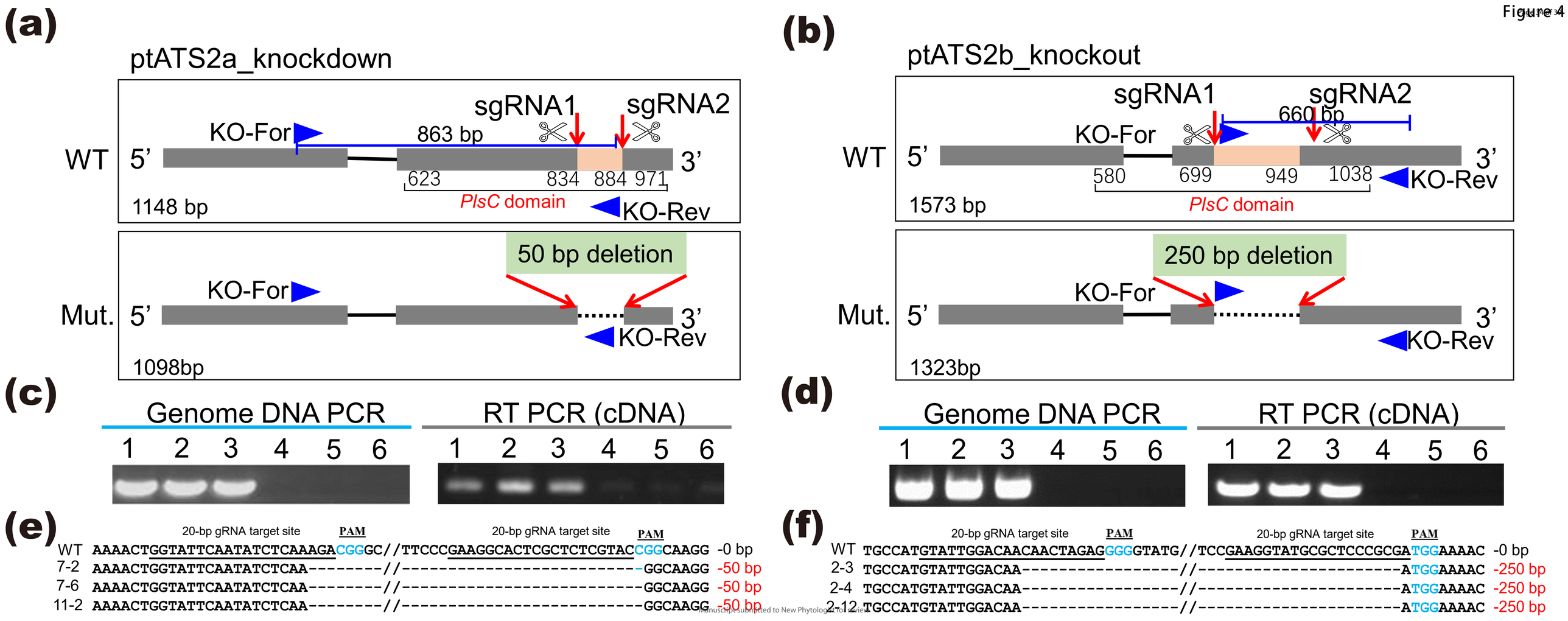

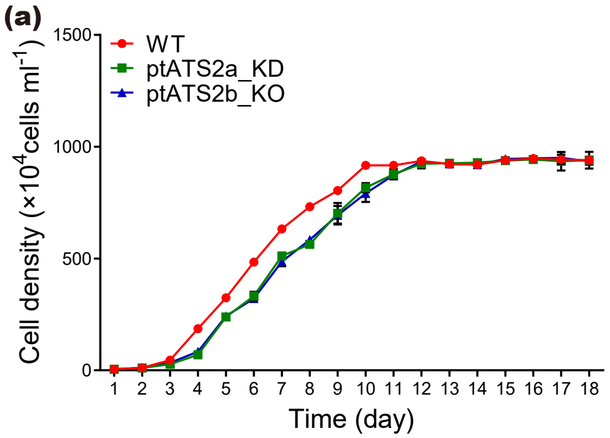

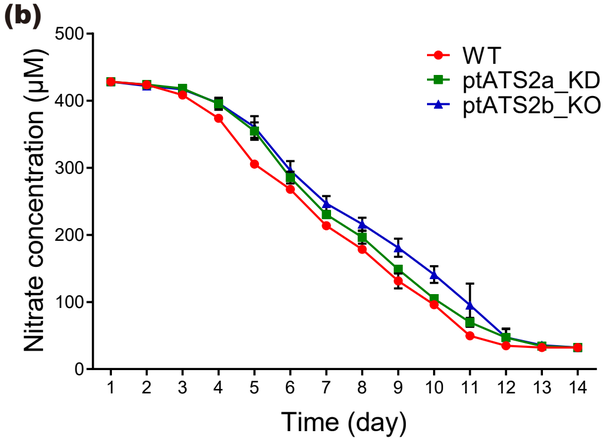

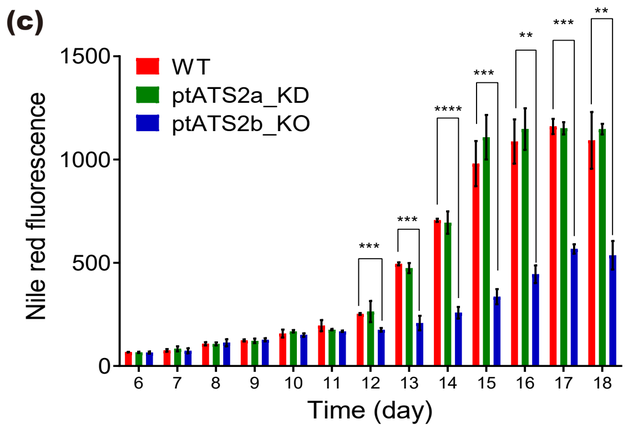

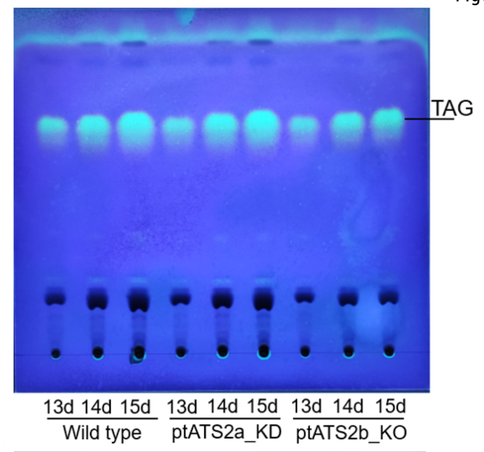

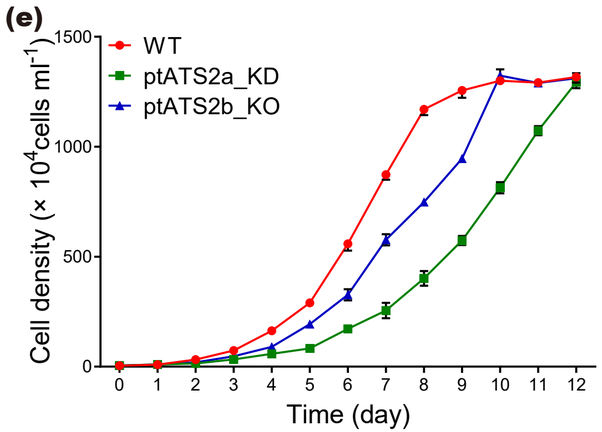

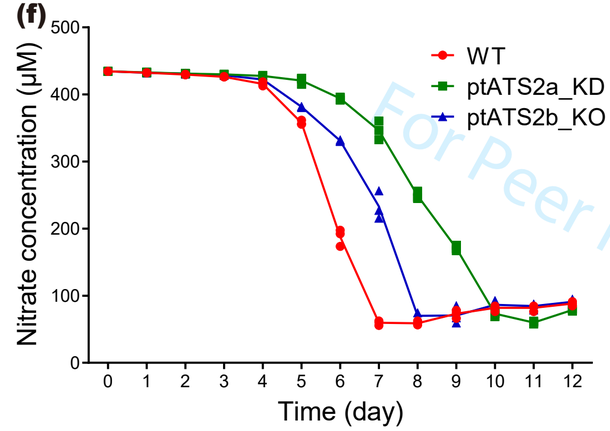

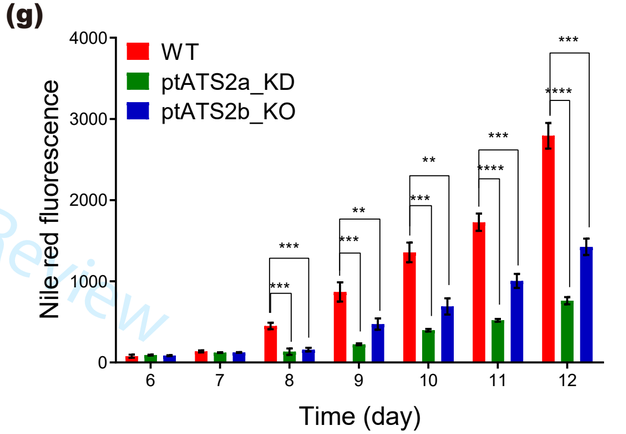

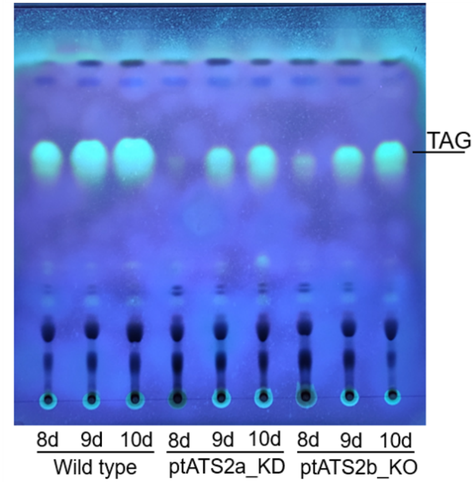

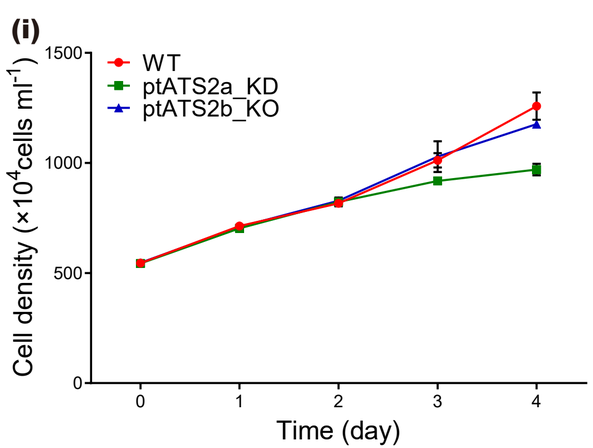

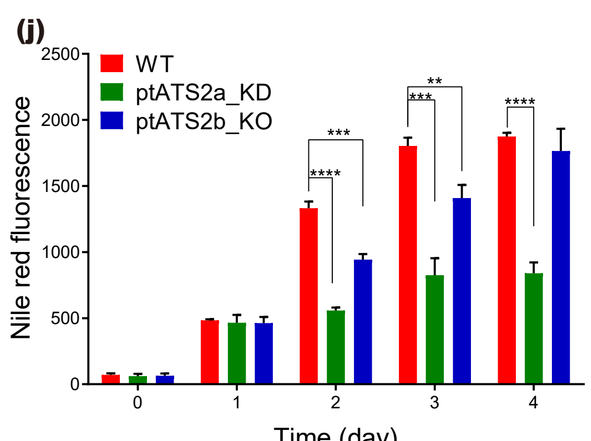

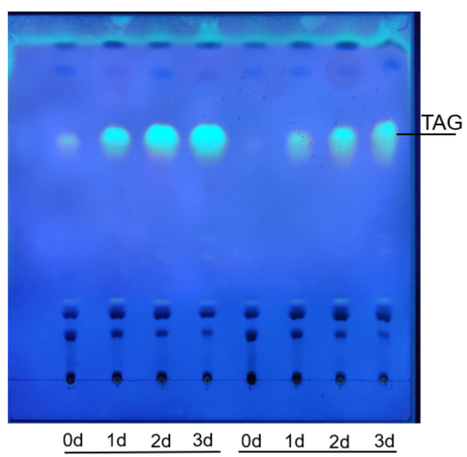

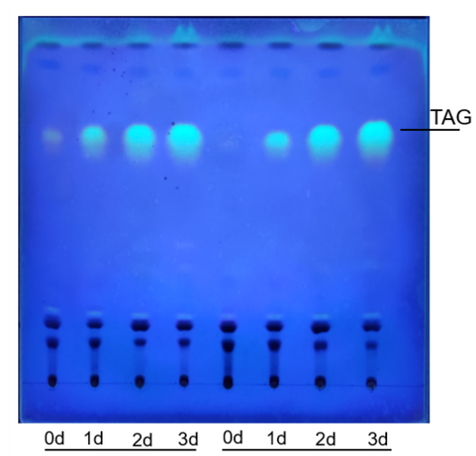

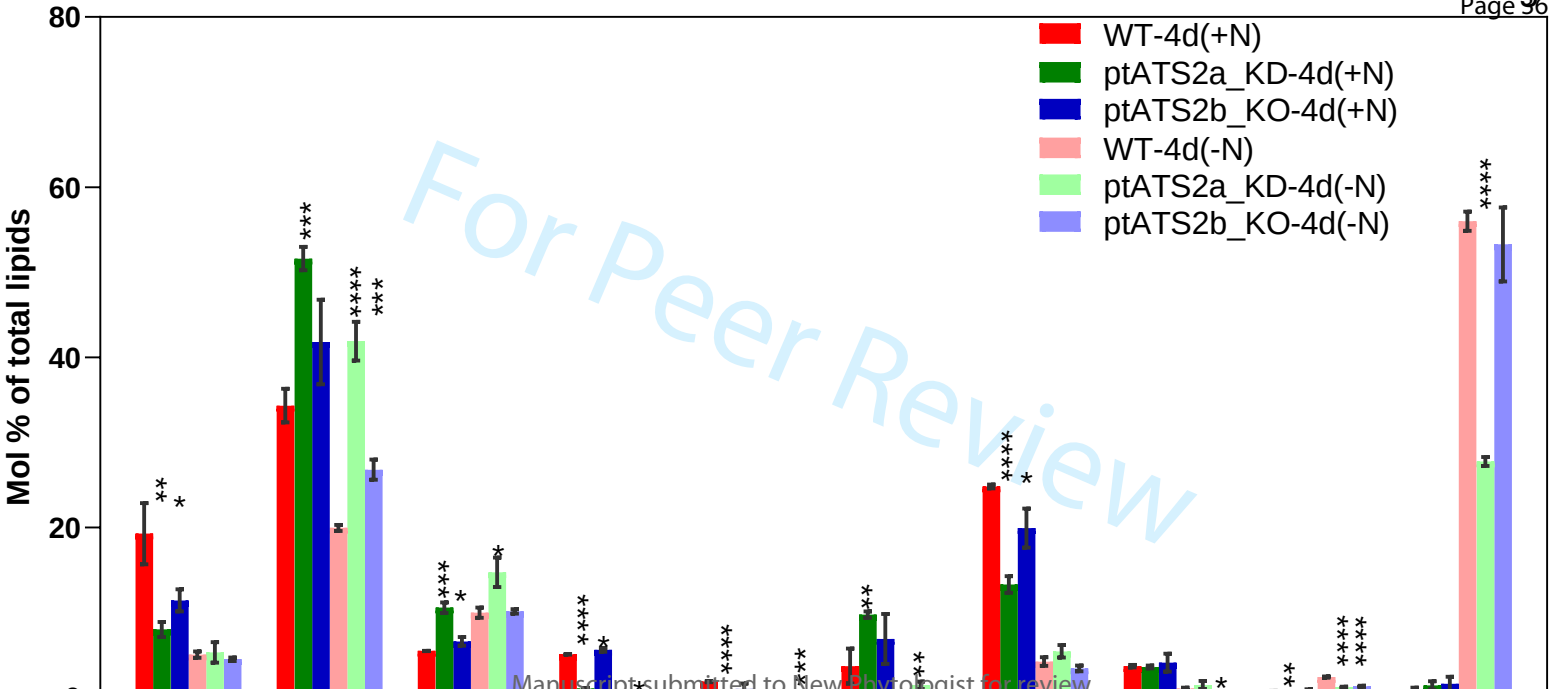

Figure 7

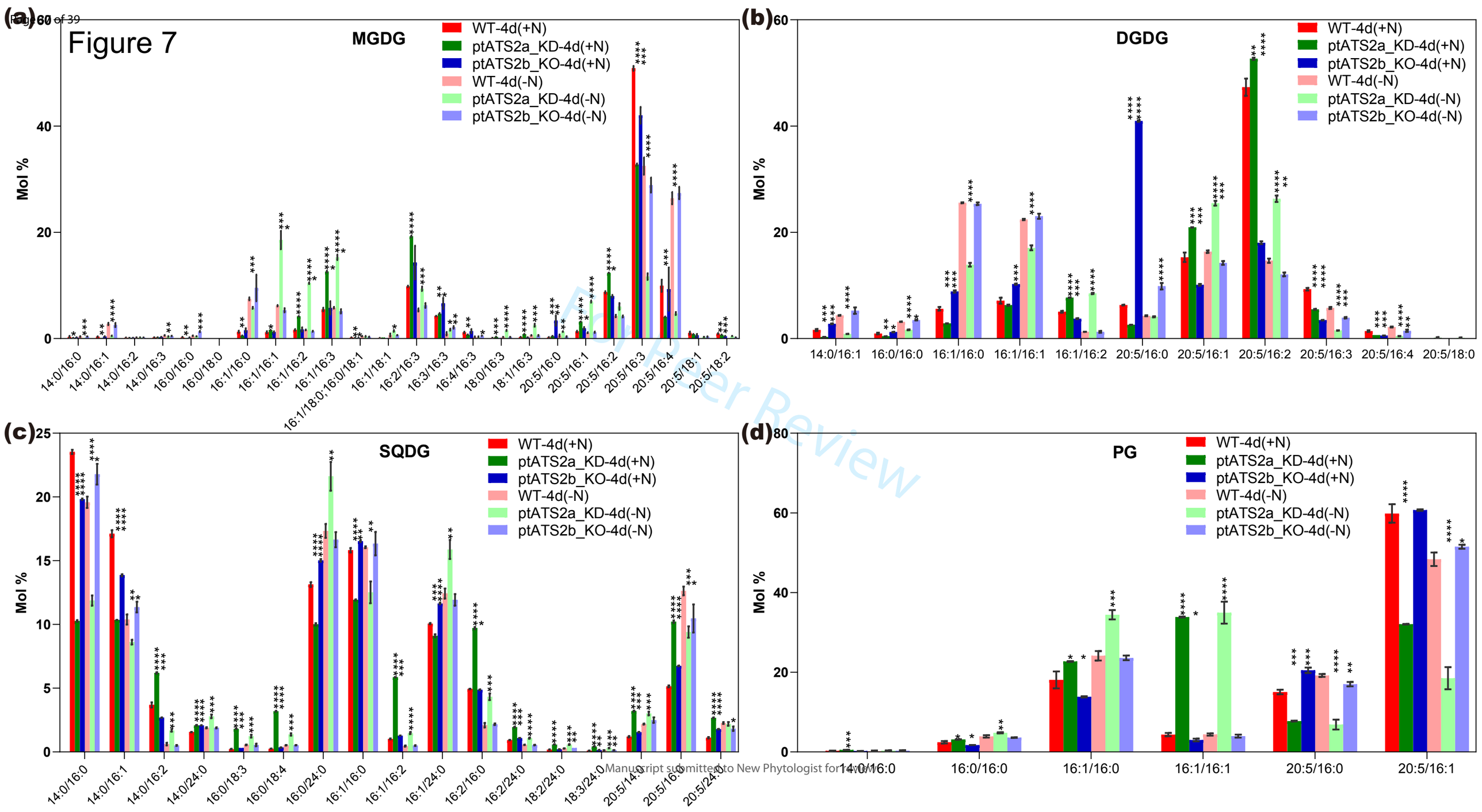

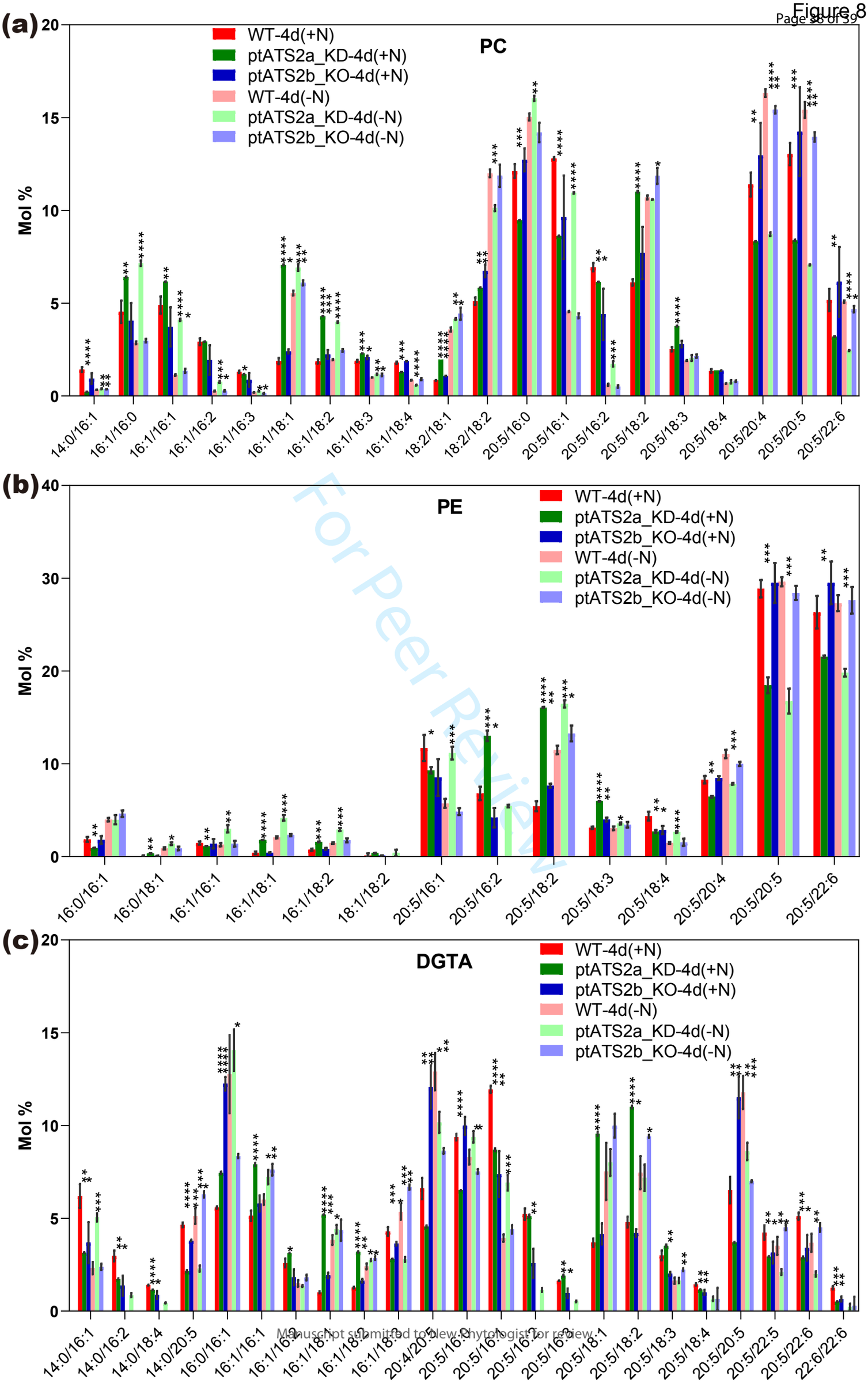

Figure 9

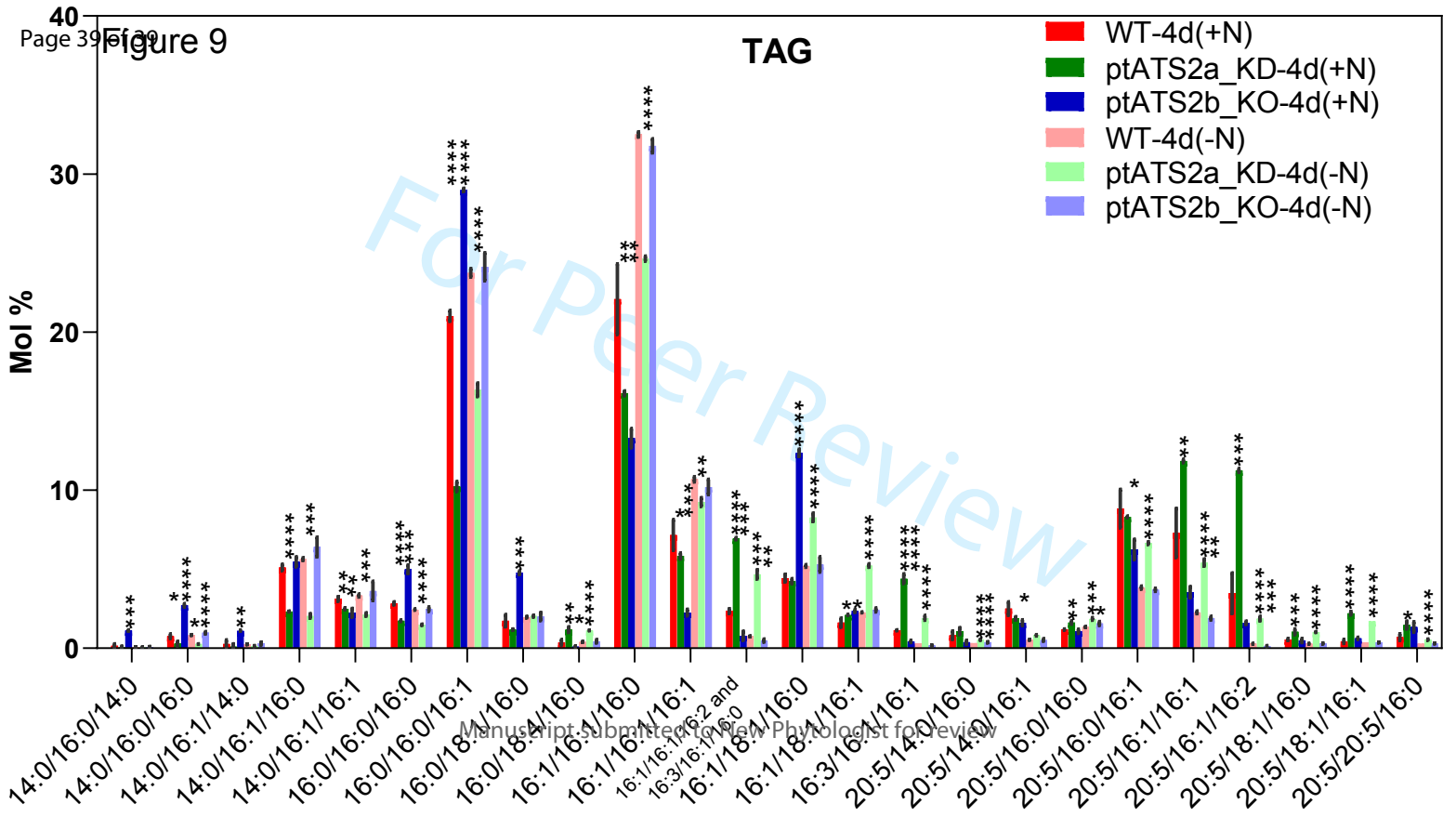

Figure 10

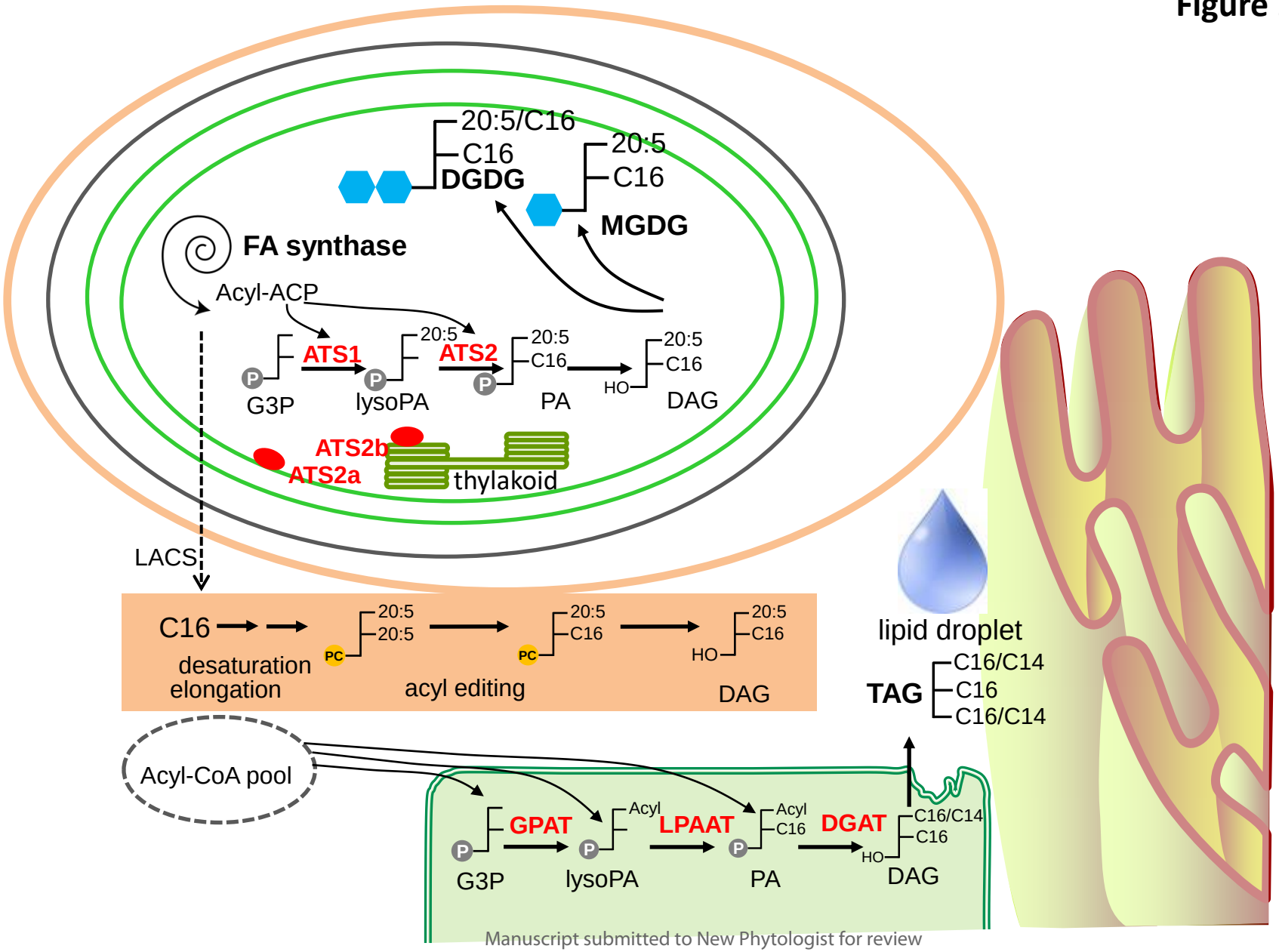
20:5/C16
C16
DGDG
20:5
C16
MGDG
FA synthase
Acyl-ACP
ATS1
ATS2
20:5
20:5
C16
20:5
C16
HO
G3P
lysoPA
PA
DAG
ATS2b
ATS2a
thylakoid
LACS
C16
desaturation
elongation
20:5
20:5
PC
20:5
C16
PC
acyl editing
HO
20:5
C16
DAG
lipid droplet
TAG
C16/C14
C16
C16/C14
Acyl-CoA pool
GPAT
LPAAT
DGAT
Acyl
Acyl
C16
C16/C14
C16
HO
G3P
lysoPA
PA
DAG